Atmospheric methane isotopes identify inventory knowledge gaps in the Surat Basin, Australia, coal seam gas and agricultural regions

Bryce F. J. Kelly[1] Xinyi Lu[1], Stephen J. Harris[1], Bruno G. Neininger[2], Jorg M. Hacker[3,4], Stefan Schwietzke[5], Rebecca E. Fisher[6], James L. France[5,6], Euan G. Nisbet[6], David Lowry[6], Carina van der

5   Veen[7], Malika Menoud[7], Thomas Röckmann[7].

[1]School of Biological, Earth and Environmental Sciences, The University of New South Wales (UNSW Sydney), NSW, 2052, Australia
[2]MetAir AG, Airfield LSZN, Switzerland
[3]Airborne Research Australia, Parafield Airport, SA, 5106, Australia
10   [4]College of Science and Engineering, Flinders University, SA, 5001, Australia
[5]Environmental Defense Fund, Third Floor, 41 Eastcheap, London, EC3M 1DT, United Kingdom
[6]Department of Earth Sciences, Royal Holloway, University of London, Egham, TW20 0EX, UK
[7]Institute for Marine and Atmospheric research Utrecht (IMAU), Utrecht University, Utrecht, 3584 CC, the Netherlands

Correspondence to: Bryce F. J. Kelly (bryce.kelly@unsw.edu.au)

Abstract

In-flight measurements of atmospheric methane ($CH_{4(a)}$) and mass balance flux quantification studies can assist with verification and improvement of UNFCCC National Inventory reported CH_4 emissions. However, attributing $CH_{4(a)}$ mole fraction readings to one or more emission sources is difficult where co-located plumes mix rapidly within the convective boundary layer. The stable carbon isotopic signatures of CH_4 sources can assist with source attribution and potentially identify bottom-up (BU) inventory knowledge gaps and identify mitigation opportunities. In the Surat Basin, Queensland, Australia, both coal seam gas (CSG) production and cattle farming are increasing sources of CH_4 emissions into the atmosphere. The CSG fields cover thousands of square kilometres and many CSG facilities and farms are inaccessible as part of ground-based surveys.

The aims of this study were to explore the use of $CH_{4(a)}$ isotopic composition ($\delta^{13}C_{CH4(a)}$) of in-flight atmospheric air (IFAA) samples and the application of source endmember mixing models to assess where the BU inventory was well characterised, to identify potential gaps in the BU regional inventory (missing sources, or over- and underestimation source categories), identify mitigation opportunities, and to characterise the isotopic signature of CH_4 sources that were inaccessible during ground surveys. Forty-nine useable IFAA samples were collected between 100–350 m above ground level (mAGL) over a region of CSG, coal mining and agricultural production over a 2-week period in September 2018. For each IFAA sample the 2-hour back trajectory footprint area was determined using the NOAA HYSPLIT atmospheric trajectory modelling application. Samples were then assigned to a source category set where over 50 % of the 2-hour upwind BU inventory could be attributed to a single source (CSG, grazing cattle, or feedlots), and further differentiated based on altitude (100–200 mAGL or 250–350 mAGL). A novel multi-dataset (source category) regression method with shared parameters (background air $CH_{4(b)}$ and $\delta^{13}C_{CH4(b)}$) was used to fit Keeling models simultaneously to each data set. The determination of a common background endmember ($CH_{4(b)}$ and $\delta^{13}C_{CH4(b)}$) for the two-endmember mixing model reduces the uncertainty in the derived isotopic signature for a source ($\delta^{13}C_{CH4(s)}$). The estimated $\delta^{13}C_{CH4(s)}$ signatures for each category were then compared to the database of source $\delta^{13}C_{CH4(s)}$ signatures established from ground studies.

For IFAA samples collected between 250–350 mAGL altitude, the best-fit $\delta^{13}C_{CH4(s)}$ signatures compare well with the ground observation: CSG $\delta^{13}C_{CH4(s)}$ −55.5 ‰ (CI 95 % ± 13.4 ‰) versus $\delta^{13}C_{CH4(s)}$ −56.7 ‰ to −45.6 ‰; grazing cattle $\delta^{13}C_{CH4(s)}$ −60.5 ‰ (CI 95 % ± 15.1 ‰) versus −61.7 ‰ to −57.5 ‰. For feedlots, the derived $\delta^{13}C_{CH4(s)}$, −69.5 ‰ (CI 95 % ± 22.1 ‰), was isotopically lighter than the ground-based study ($\delta^{13}C_{CH4(s)}$ from −65.2 ‰ to −60.3 ‰), but within agreement given the large uncertainty for this source. For IFAA samples collected between 100–200 mAGL the $\delta^{13}C_{CH4(s)}$ signature for the CSG set, −65.3 ‰ (CI 95 % ±13.1 ‰), was isotopically lighter than expected, suggesting a BU inventory knowledge gap or the need to extend the population statistics for CSG $\delta^{13}C_{CH4(s)}$ signatures. For the 100–200 mAGL set collected over grazing cattle districts the $\delta^{13}C_{CH4(s)}$ signature, −52.5 ‰ (CI 95 % ± 18.8 ‰), was much heavier than expected from the BU inventory. This is likely due to CSG CH_4 emissions entering the study domain from an adjacent CSG field. Using the multi-Keeling-model regression derived background air values (1.825 ppm (CI 95 % ± 0.037 ppm) and −47.3 ‰ (CI 95 % ± 0.3 ‰)), a Keeling model fitted to the isotopically light set yielded a low $\delta^{13}C_{CH4(s)}$ signature of −80.5 ‰ (CI 95 % ± 9.2 ‰). A CH_4 source with this low $\delta^{13}C_{CH4(s)}$ signature and a high rate of emissions has not been incorporated into existing BU inventories for the region. Further ground-based studies are required to identify the isotopically light CH_4 source, with possible sources including termites and CSG brine ponds. If the excess emissions are from the brine ponds, they can be abated. It is concluded that in-flight atmospheric $\delta^{13}C_{CH4(a)}$ measurements used in conjunction with endmember mixing modelling of CH_4 sources are powerful tools for BU inventory verification and for identifying sources that can be mitigated. The subregions identified for BU inventory review would likely have been overlooked based on $CH_{4(a)}$ measurements alone.

1 Introduction

60   There is considerable international interest in mapping and mitigating sources of CH_4, because it is a potent greenhouse gas. This is reflected by the fact that over 100 countries signed the international CH_4 pledge launched at COP26 in November 2021, which aims to strengthen support for CH_4 emission reduction initiatives (https://www.globalmethanepledge.org/). Currently there are plans to expand coal seam gas and shale gas productions throughout many regions of Australia (Australian Government, 2021); thus it is critical to understand how this expansion will contribute to regional, national and global

65   emissions. We also need to improve our knowledge of greenhouse gas emissions from agricultural districts. This study uses methane (CH_4) carbon isotopic composition ($\delta^{13}C_{CH4}$) to gain additional insights into coal seam gas (CSG; refer to Table A1 for a listing of abbreviations), coal mining and agricultural contributions to regional and global atmospheric emissions. We also demonstrate how atmospheric isotope studies can identify mitigation opportunities.

70   The southeast portion of the Surat Basin, Queensland, Australia is an area of approximately 200 km by 200 km, where there are over 4,000 producing CSG wells, active and inactive open-pit coal mines, piggeries, and millions of cattle in feedlots and grazing throughout the mixed agricultural districts. The study area covers approximately 0.5 % of Australia yet produces 3–4 % of Australia's CH_4 emissions (Australian Government, 2020a, 2020b; Neininger et al. 2021). Other CH_4 sources close to CSG production in the Surat Basin include domestic wood heaters, landfills, wastewater treatment plants, and natural seeps

75   from the Condamine River. The rapid expansion of CSG in the south-eastern region of the Surat Basin has resulted in considerable research interest in quantifying the emissions from the CSG sector. A review of all past ground-based CH_4 surveys in the region is presented in Lu et al. (2021).

The Australian Government has developed its own methods for estimating emissions from CSG facilities (Australian

80   Government, 2020b, Neininger et al. 2021). Because of Australia's unique climate and farming practices there are many locally approved emission factors for agricultural sources and methods for determining regional emissions (Australian Government, 2020b; EFDB, 2006; IPCC, 2006, 2019). To support the CH_4 studies in the Surat Basin a BU inventory was calculated for the region using the methods outlined in Australia's 2018 National Inventory submission to the UNFCCC (Australian Government, 2020a). The comprehensive details about that inventory and the data sets used are discussed at length in Neininger et al. (2021).

85   In the past decade there has been increased use of top-down (TD) airborne and satellite measurements to verify BU inventories (Barkley et al., 2017; Gorchov Negron et al., 2020; Karion et al., 2013, 2015; Neininger et al., 2021; Peischl et al., 2015, 2016, 2018; Pétron et al., 2014; Schwietzke et al., 2017; Turner et al., 2015; Yacovitch et al., 2018; Zhang et al., 2020, 2021). Previous studies have shown that it is not uncommon to find a large difference between BU inventory versus TD estimates of emissions (Kirschke et al., 2013; Desjardins et al. 2018; Saunois et al., 2020). Much of this uncertainty is due to the quality

90   and resolution of the base data sets used for calculating the emissions (Han et al., 2020; Verhulst et al., 2017).

In 2018 and 2019 CH_4 emissions from many facilities were mapped using a car-mounted Los Gatos Research ultraportable greenhouse gas analyser (Los Gatos Research, Inc., USA). Where CH_4 plumes were detected and the source identifiable, the air was sampled and analysed to determine the isotopic signature for the CH_4 source (Lu et al. 2021; Table A2). In conjunction

95   with the ground surveying, in September 2018 an airborne survey of CH_4 emissions was undertaken (Neininger et al. 2021), the focus of which was regional and sub-regional CH_4 mass balance analyses. An exploratory component of the study was to collect in-flight atmospheric air (IFAA) samples to assess whether additional insights about CH_4 sources could be obtained from analysing $\delta^{13}C_{CH4}$. It was also envisaged that the $\delta^{13}C_{CH4}$ measurements would yield additional insights into over- and underestimated sources of CH_4 in the bottom-up (BU) inventory developed for the mass balance study (Neininger et al. 2021).

100   The focus of the investigation was primarily to improve our understanding of CH_4 emissions from CSG production. However,

many of the CSG facilities are co-located with feedlots, piggeries, and grazing cattle, thus we investigated all sources (Lu et al. 2021, Neininger et al. 2021).

105 The aims of this study were to use the measurement of $CH_{4(a)}$ mole fraction and $\delta^{13}C_{CH4(a)}$ in 49 IFAA samples and endmember mixing modelling to assess the quality of the regional BU inventory (missing sources, or over- and underestimation source categories). An additional aim was to extend our knowledge of the $\delta^{13}C_{CH4}$ population statistics of CH_4 sources in the region for CH_4 sources that were inaccessible during ground surveys. We also used the measurements to identify mitigation opportunities and to identify where more detailed CH_4 emission source studies are required.

110 For CH_4 emission studies both carbon ($\delta^{13}C$) and hydrogen (δD) isotopic composition can help with determining CH_4 sources and the extent of mixing of various sources (Lowry et al., 2020; Menoud et al., 2020; Menoud et al., 2021; Röckmann et al., 2016; Townsend-Small et al., 2015), but in this study only $\delta^{13}C$ is used. Due to the population range in $\delta^{13}C_{CH4}$ values for each source, $\delta^{13}C_{CH4}$ may or may not be useful for source attribution (Lan et al., 2021; Lu et al., 2021; Milkov and Etiope, 2018; Menoud et al. 2022a; Quay et al., 1999; Sherwood et al., 2017, 2020). Thus, the interpretation of IFAA sample $\delta^{13}C_{CH4(a)}$ must be examined critically in the context of likely sources documented in the BU inventory upwind of a sample collection point.
115 In other methane emission studies focused on the gas sector, ethane has been used for fossil fuel attribution (Smith et al. 2015; Johnson et al. 2017; Mielke-Maday et al. 2019). However, in the Surat Basin ethane is not a useful tracer because the ethane content of the produced gas is less than 1 % (Hamilton et al. 2012; Sherwood et al. 2017).

The mixed source $\delta^{13}C_{CH4(a)}$ value of an IFAA sample can be used to provide insights into what CH_4 sources should be in an upwind inventory (Lowry et al., 2020; Menoud et al., 2022b; Townsend-Small et al., 2015; Worden et al., 2017; Zazzeri et al.,
120 2017). When used together, TD airborne measurements and source tracers provide constrained estimates for each source of CH_4 and its contribution to the overall emissions (Beck et al., 2012; Fisher et al., 2017; France et al., 2016; Tarasova et al., 2006). Using IFAA sampling to characterise the $\delta^{13}C_{CH4(s)}$ signatures of CH_4 sources has many challenges. There are often numerous CH_4 sources upwind; it takes time to fill the sample collection bags (resulting in a sampling window in the order of kilometres); assumptions must be made about the mixing of air parcels within the convective boundary layer; and it is often
125 not possible to sample enough points to minimise the uncertainty of $\delta^{13}C_{CH4(s)}$ signature estimates.

Assumptions must also be made about the uniformity of emissions from all CH_4 sources. A good BU inventory can help to minimise some of these issues. However, BU inventories can contain errors. Sources of CH_4 may have been overlooked when collating the inventory, or individual CH_4 sources may have been over- or underestimated. Thus, there is two-way feedback.
130 The IFAA samples provide insights into what is expected in the upwind BU inventory, and the BU inventory guides what is expected in the IFAA samples.

On warm days the plumes for each CH_4 source rise rapidly and mix within the convective boundary layer with incoming regional background air. Sampling flights were restricted to when the convective boundary layer was greater than 1000 mAGL
135 and before the vertical mixing was suppressed and the top of the convective boundary layer not definable (Neininger et al. 2021). This mixing of both the relatively small CH_4 point and diffuse sources with incoming low mole fraction CH_4 background air within the large volume of the convective boundary layer reduces the CH_4 enhancement over background to less than 0.1 ppm, often to the order of 0.01 ppm. The low CH_4 enhancement also makes it difficult to distinguish CH_4 sources with isotope techniques where air samples are collected over regions with multiple source categories. Given these challenges, and the spatial
140 and temporal variability of CH_4 emissions in regions of complex industrial and agricultural production, it is improbable that BU inventories will exactly match TD estimates of CH_4 emissions. An IFAA sample should contain a blend of all sources of

CH₄ immediately upwind of the sample in proportion to the source strength and rate of mixing with incoming background air (the well-mixed air within the convective boundary layer entering a region).

145 A well-established method to determine the $\delta^{13}C_{CH4(s)}$ signature is to collect air samples within the plume downwind of the source and analyse the data using a two-endmember mixing model (Keeling, 1961; Pataki et al., 2003; Miller and Tans 2003). The airborne surveys were not designed to track individual plumes; the flight tracks were designed to optimise the results for regional mass balance estimates of CH₄ emissions (Neininger et al. 2021). However, multiple IFAA samples were collected downwind of a single source category, for example CSG or cattle feedlots, and these samples were analysed in sets, which is

150 analogous to multiple samples in a plume. One aim of this study was to examine the $\delta^{13}C_{CH4(s)}$ signature of regions with common source categories. Upwind sources were identified from the BU inventory presented in Neininger et al. (2021). Hybrid single particle Lagrangian integrated trajectory (HYSPLIT) modelling (Draxler et al., 1998) was used to determine the 2-hour back-trajectory footprint (BTF). The IFAA sample $\delta^{13}C_{CH4(a)}$ was then analysed in the context of the 2-hour BTF BU inventory, as sources within this time interval were demonstrated in Neininger et al. (2021) to contribute significantly to the measured

155 CH₄ along each flight track (refer to Neininger et al. (2021) supplementary material Figure SF26 for an example of the more detailed back trajectory modelling, used to guide the HYSPLIT settings).

In this study multi-Keeling-model regression with shared parameters (background air CH₄(b) and $\delta^{13}C_{CH4(b)}$) is used to analyse the IFAA samples. This methodology enables robust characterisation of CH₄(b) and $\delta^{13}C_{CH4(b)}$, verification of the isotopic

160 signatures of known sources, and the identification of sources of CH₄ overlooked in BU inventories. We show that these insights highlight where further research is required to improve the Surat Basin regional BU inventory and the methods used for UNFCCC reporting.

2 Materials and methods

2.1 Overview of the study area

165 The study area is in the Condamine natural resource management region of southeast Surat Basin, Queensland (Fig. 1 (a)). It includes the southeast portion of the Surat Basin CSG field, which is the largest CSG producing field in Australia with more than 60 % of Australia's total proven gas reserves (Australian Competition and Consumer Commission, 2020). The CSG is primarily produced from coals with high permeability in the middle Walloon Coal Measures (Baublys et al., 2015; Draper and Boreham, 2006; Scott et al., 2007). In the CSG field there are numerous CH₄ emission sources including CSG wells

170 (exploration, appraisal, production and abandoned), field compression stations, central processing plants, gas and water transmission pipelines and raw water ponds (CSG co-produced water storage) (Fig. 1 (b)). CH₄ emitted from agricultural activities is another major source of atmospheric emissions. Grazing cattle herds and beef or dairy feedlots are spread throughout the study area, and grazing cattle and feedlots are often adjacent to CSG infrastructure (Fig. 1 (b)). There is also stored animal waste associated with the cattle feedlots and piggeries. Known but poorly quantified sources of CH₄ in the study

175 area include bush fires, wetlands, termites, on-farm biosolid fertilisers, emissions from un-capped coal and gas exploration wells, and emissions from an abandoned coal gasification development (Lu et al., 2021).

To support the airborne mass balance estimate of CH₄ emissions presented in Neininger et al. (2021), the University of New South Wales (UNSW) prepared a BU inventory for 2018, and comprehensive details of this inventory are provided in Neininger

180 et al. (2021). The UNSW BU inventory is larger than the region within which the IFAA samples were collected (Fig. 1) to allow comparison between the IFAA sample and the upwind BU inventory. The IFAA samples are referenced using a four-

number string: the first two numbers are the day in September 2018, and the second two numbers are the sample reference for the day. A full listing of the IFAA samples and their sample location details are presented in Table A3.
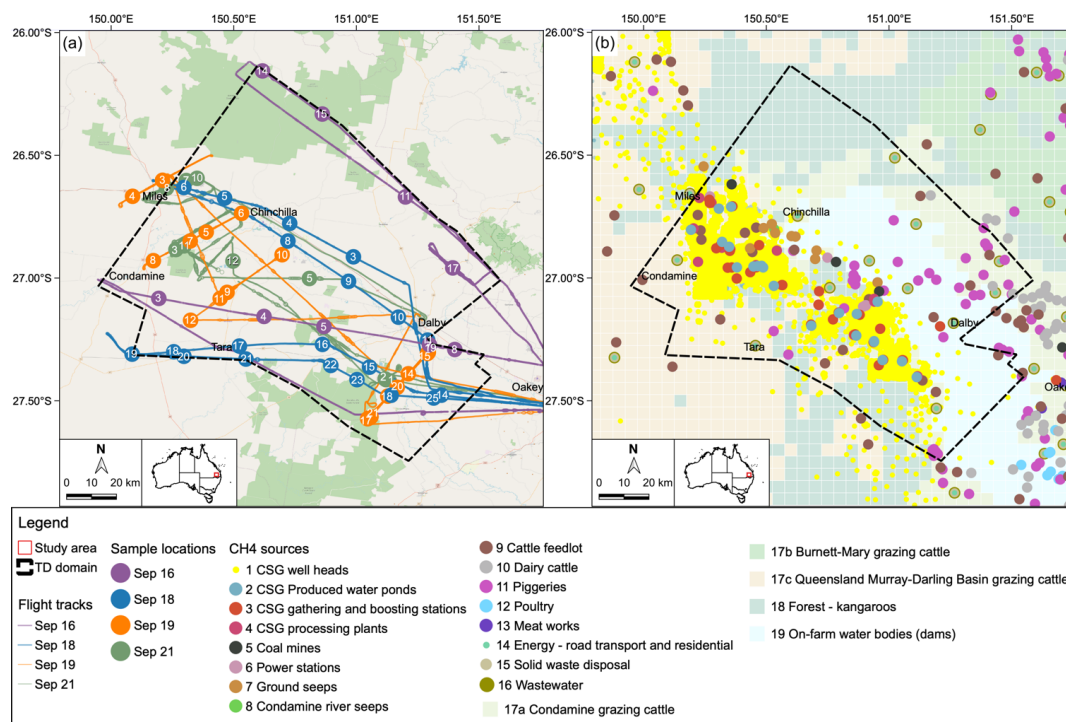
Figure 1. Map of the study area with flight tracks and in-flight atmospheric air (IFAA) sample locations (a) (inset map shows the location in south-eastern Queensland) and map of the CH₄ sources in the area (b). (Inset map data: Australian Government (2020), Administrative Boundaries © Geoscape Australia. Base map and data from OpenStreetMap and OpenStreetMap Foundation).

2.2 BU and TD CH₄ emission estimates in the Surat Basin

The UNSW BU inventory closely followed the methods outlined in Australia's 2018 National Greenhouse Gas Inventory (Australian Government, 2020a). The UNSW inventory covers known sources such as those from the CSG industry and agriculture as well as sources discovered during the 2018 ground campaign in the study area (Lu et al., 2021). The inventory was collated using publicly available data. These data were supplemented with information from environmental impact approval reports, government and industry documents, close inspection of the satellite imagery in Google Earth, and airborne and ground survey observations (discussed in Lu et al., 2021 and Neininger et al., 2021). The locations of the sources contained in the UNSW inventory are shown in Fig. 1 (b).

In Fig. 2 (a) all point sources are presented as an emission intensity map, and in Fig. 2 (b) the distributed sources are shown. CSG sources are concentrated in a northwest to southeast zone, with agricultural sources on either side. The UNSW inventory estimate for the CH₄ emissions in the southeast portion of the Surat Basin CSG fields for 2018 is 20,900 kg h⁻¹ (183 Gg yr⁻¹). In the UNSW inventory most of the emissions come from cattle, which contribute 50.3 % (29.9 % from grazing cattle, 19.1 % from feedlots, and 1.3 % from dairy cattle); all CSG sources contribute 30.5 %, piggeries 8.7 %, coal mines 7.6 %, and all other sources contribute only 2.9 %. Within the airborne measurement TD domain, the UNSW inventory estimate for CH₄ emissions is 11,500 kg h⁻¹ (101 Gg y⁻¹), and the percentage contribution order within the TD domain is different: CSG 53.7 %, feedlots 19.0 %, grazing cattle 14.1 %, piggeries 7.3 %, coal 3.5 %, and all other sources 2.4 %. The heterogeneity of the point source emission rate is visually apparent in Fig. 2 (a). Within the UNSW inventory domain, 50 % of point sources have

an emission rate of less than 4.5 kg h⁻¹. These point sources account for 59 % of the UNSW inventory total. The top 10 % have an emission rate exceeding 113 kg h⁻¹. The 42 sources in the top 10 % account for 37.7 % of the UNSW inventory total. The largest individual source is an open-pit coal mine (27.28° S, 151.71° E), which emits 843 kg h⁻¹ (4.1 % of the UNSW

210 inventory total). The second largest source is a feedlot (27.42° S, long. 151.14° E), which emits 563 kg h⁻¹ (2.7 % of the UNSW inventory total). The largest CSG source is a raw water pond (26.96° S, 150.49° E), which emits 221 kg h⁻¹ (1.1 % of the UNSW inventory total).

The distributed sources of CH₄ are dominated by grazing cattle (dark red in Fig. 2 (b), 6.54 kg h⁻¹ per 25 km²), followed by

215 the irrigation farming district (light blue, 0.64 kg h⁻¹ per 25 km²), and then the forested areas with kangaroos (purple, 0.09 kg h⁻¹ per 25 km²). There may also be some termite emissions from the forested areas, but these have not been quantified. Grazing cattle account for 29.9 % of the UNSW inventory total CH₄ emissions. The position of this large source of CH₄ emissions is one of the largest uncertainties in the calculations below. To maintain soil health and grass cover the grazing cattle are rotated through various fields, and at times the cattle also graze along the roadside. The forested areas with large kangaroo populations

220 were estimated to contribute only 0.2 % of all CH₄ emissions. The irrigated agricultural district was estimated to have diffuse CH₄ emission sources contributing only 0.7 % towards the UNSW inventory total.

Using airborne measurement techniques, Neininger et al. (2021) quantified the CH₄ emissions in the south-eastern portion of the Surat Basin CSG fields and surrounding agricultural districts. In the September 2018 campaign, there were 10 flights (∼

225 45 h) using a research motorglider operated by Airborne Research Australia (ARA). Neininger et al. (2021) showed that there was strong correlation between the TD CH₄ flux estimate and the UNSW inventory. Within the airborne survey domain, the TD estimate was 13,500 kg h⁻¹ (118 Gg yr⁻¹), which is 1,940 kg h⁻¹ (17 Gg yr⁻¹) higher than the UNSW inventory.
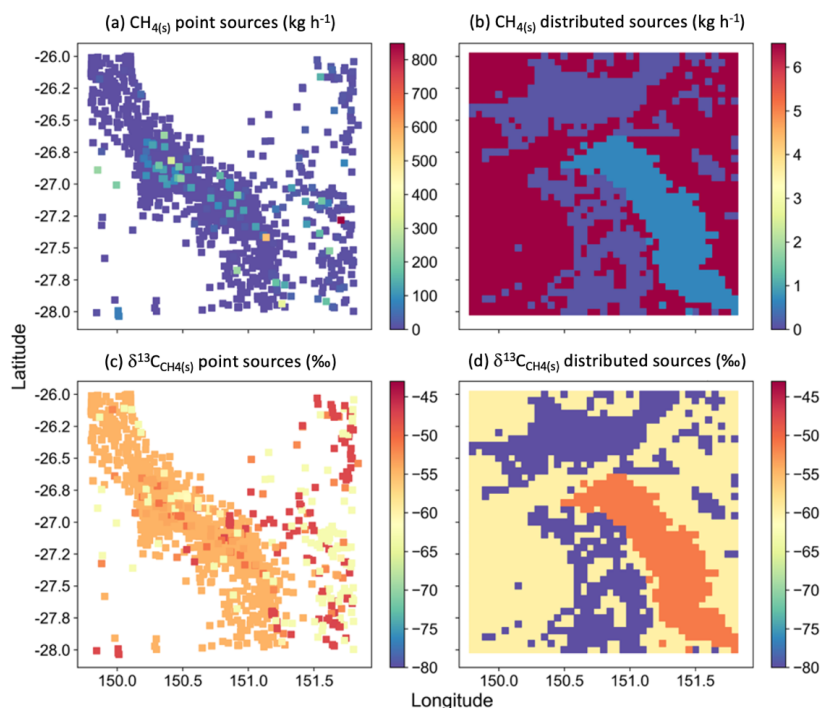
230 **Figure 2.** Maps of the UNSW BU inventory (5 × 5 km for each grid cell) in the southeast portion of the Surat Basin CSG fields showing the estimated CH₄(s) emissions for point (a) and distributed (b) sources and assigned δ¹³C_CH4(s) for point (c) and distributed (d) sources.

2.3 $\delta^{13}C_{CH4(s)}$ for each inventory category

The, $\delta^{13}C_{CH4(s)}$ of 16 primary sources in the Surat Basin were characterised in Lu et al. (2021) using air samples collected during ground-based surveys. These values are listed in Table A2 and were assigned to the different source categories in the

235   inventory to create isotopic source signature maps. The spatial locations of the CH$_4$ point sources and their corresponding $\delta^{13}C_{CH4(s)}$ values are shown in Figs 2 (a) and 2 (c). The distribution of the CH$_4$ diffuse sources and corresponding $\delta^{13}C_{CH4(s)}$ values are shown in Figs. 2 (b) and 2 (d). For many source types only one $\delta^{13}C_{CH4(s)}$ signature was determined in Lu et al. (2021). Gaining access to a wide range of farms and CSG facilities is difficult due to operational procedures, and health and safety concerns. Therefore, an aim of this study was to examine if IFAA samples can be used to extend our knowledge of the

240   CH$_{4(s)}$ signatures from various sources in the Surat Basin.

From the ground-based studies, the $\delta^{13}C_{CH4(s)}$ signatures from CSG processing and production facilities and CSG raw water ponds ranged from −56.7 ‰ to −45.6 ‰ (Bayesian 95 % credible interval (CrI); Lu et al. 2021). CSG is extracted from a range of depths in the Surat Basin gas fields. The shallowest coal measures tend to have a lighter isotopic signature and the deeper

245   coal measures a heavier signature. The reported range for $\delta^{13}C_{CH4(s)}$ from gas from the Walloon Coal Measures is −64.1 ‰ to −44.5 ‰ (Baublys et al., 2015; Draper and Boreham, 2006; Hamilton et al., 2014, 2015; Iverach et al. 2015, 2017; Stalker and Smith, 2004). The difference between the ground-based studies and well observations highlight the need to better characterise $\delta^{13}C_{CH4(s)}$ population statistics of CSG and other CH$_4$ sources.

250   In addition to CSG sources of CH$_4$ there are four major sources of CH$_4$: feedlots, grazing cattle, piggeries, and coal mines (Neininger et al. 2021). For each of these sources only a single plume has been sampled to estimate $\delta^{13}C_{CH4(s)}$, thus many more data sets need to be collected to robustly define the population statistics. A useful measure for the likely range of $\delta^{13}C_{CH4(s}$ for each source category is summarised by the $\delta^{13}C_{CH4(s)}$ Bayesian CrI, which for the limited sampling to date are: feedlots, −65.2 ‰ to −60.3 ‰; grazing cattle, −61.7 ‰ to −57.5 ‰; piggeries −48.0 ‰ to −47.1 ‰, and coal mines, −61.1 ‰ to −58.9 ‰.

255   Refer to Lu et al. (2021) for comprehensive details about how these isotopic signatures were determined and details about Bayesian regression.

In the study area two smaller sources of CH$_4$ have both the lowest (−80 ‰ (kangaroos; Godwin et al., 2014)), and the highest $\delta^{13}C_{CH4(s)}$ value (−22.2 ‰ (biomass burning; Ginty, 2016)). There are also numerous termite mounds in the region, but there

260   have been no studies on the rate of CH$_4$ emissions from these mounds, nor has $\delta^{13}C_{CH4(s)}$ been characterised for termites in the region.

For CH$_4$ source categories listed in the BU inventories that were not sampled during the mobile survey, $\delta^{13}C_{CH4(s)}$ signatures were obtained from the literature. These include the $\delta^{13}C_{CH4(s)}$ signatures for kangaroos (Godwin et al., 2014), on-farm water

265   bodies (dams) (Day et al., 2016), domestic wood heaters and native vegetation wildfires (Ginty, 2016). A major gas distribution line passes through the region; this transports conventional gas from the fields to the west of the study area to the LNG terminals on the coast and for the domestic market at Brisbane (Jemena, 2021). The $\delta^{13}C_{CH4(s)}$ population statistics for this gas are not known.

2.4 Research aircraft instrumentation and collection of the IFAA samples

270   Collecting IFAA samples in FlexFoil or similar bags is a comparatively fast and cost-effective method and has been used in numerous airborne and ground-based CH$_4$ studies (Fisher et al., 2017; France et al., 2021; Lowry et al., 2020, Menoud et al., 2022). During the campaign in September 2018, 92 IFAA samples were collected on board a Diamond Aircraft HK36TTC

ECO-Dimona, equipped with underwing pods that housed the Los Gatos Research ultraportable greenhouse gas analyser, and the modified LiCOR Li-7500 open path gas analyser for fast CO_2 and H_2O measurements, and meteorological sensors for wind and thermodynamic parameters. Specifications of the airborne platform and instruments are described in Neininger et al. (2021). Sample bags were manually filled in the cockpit by connecting them to an air sampling tube, which had an inlet mounted far outside of the fuselage under the wing. Air was drawn into 3 L SKC FlexFoil PLUS (SKC Inc., USA) sample bags with polypropylene fittings. Ambient air was drawn from the intake with the assistance of a Viton membrane pump via PU tubing. Before opening the valve of the sampling bags, the fitting was carefully flushed to avoid sampling cockpit air. The duration of bag filling was ~ 1 min, which covers a track length of about 3 km at the flying speed of ~ 170 km/h. All IFAA samples presented in this study were collected within the convective boundary layer. During each flight, the top of the convective boundary layer was established several times by ascending and descending between the lower transects. During the surveying period, the convective boundary layer typically had an upper altitude limit ranging from 1,700 to 2,700 mAGL (Neininger et al., 2021). Most of the airborne measurement surveying for the mass balance surveying and IFAA sampling was flown at altitudes of approximately 150 mAGL and 300 mAGL (Fig. 3 (a)). IFAA samples were collected on each transect, with up to 25 samples being collected in a day. When CH_4 plumes were identified from the onboard real-time display, additional samples were collected. The IFAA sample locations for the four days analysed below are shown in Fig. 1 (a).

2.5 Calculation of the UNSW BU inventory 2-hour BTF BU inventory emissions

For each IFAA sample the BTF was calculated using the NOAA Air Resources Laboratory's (ARL) HYSPLIT model (Draxler et al., 1998) (Fig A1). HYSPLIT was used for this study because it is publicly available, enabling the methods presented here to be replicated by others. The HYSPLIT model is designed and widely used for tracking air parcel trajectories as well as calculating transport, dispersion and deposition of pollutants and hazardous materials (Stein et al., 2015). In this study, we determine the contributing CH_4 sources (from the UNSW BU inventory in Neininger et al. 2021) of an IFAA sample within a BTF based on the 2-hour HYSPLIT back-trajectory starting at the IFAA sampling height. The 2-hour period was based on the forward and inverse plume modelling in Neininger et al. (2021), which established that most of the CH_4 enhancement along a flight line could be attributed to a CH_4 source located within 2 hours, and within 0.025, 0.05 and 0.1 degrees longitude/latitude on each side of the IFAA sample collection mid-point, 1-hour and 2-hour back-trajectory locations (refer to Fig. A1 for the HYSPLIT back trajectories, and Fig. A2 for a representative BTF inventory polygon). Using the HYSPLIT BTF to determine contributing sources is an easy-to-replicate method. A more rigorous method would involve forward modelling the mixing of plumes for the prevailing meteorological conditions. Given that there are over 6,000 point and distributed CH_4 sources in the region, it is beyond the scope of this project to model the plume extending from each source. For the goal of identifying major upwind sources of CH_4, the HYSPLIT BTF results compared favourably when checked against the higher resolution local scale modelling in Neininger et al. (2021). As the wind speeds changed throughout the sampling campaign this results in a different BTF for each sample. However, as will be shown below, for the purpose of identifying inventory knowledge gaps and mitigation opportunities, the variations in the BTF land surface area analysed are not critical for this study.

2.6 IFAA sample $CH_{4(a)}$ mole fraction and $\delta^{13}C_{CH_{4(a)}}$ measurements

All CH_4 mole fractions and $\delta^{13}C_{CH_4}$ values reported below were measured in the greenhouse gas laboratory at Royal Holloway, University of London (RHUL) (Fisher et al. 2006). For quality control, the IFAA samples were analysed onsite prior to shipping to the UK using a Picarro G2201-i cavity ring–down spectrometer (CRDS) (Picarro, Inc., USA). This was done to check for contamination during transportation to RHUL. If the UNSW and RHUL CH_4 mole fraction values had a difference of greater than 1 % the samples were removed and not analysed further. Forty-nine useable IFAA samples were collected. These samples had a median CH_4 mole fraction difference of 0.4 % between the UNSW and RHUL measurements. The Picarro G2201-i used for this quality control step had been previously calibrated via an interlaboratory comparison between

Commonwealth Scientific and Industrial Research Organisation (CSIRO), UNSW and RHUL. This calibration used Southern

315 Ocean air from 2014 and 2016. Comprehensive details of the Picarro G2201-i performance are discussed in Lu et al. (2021).

To control for any potential instrument drift, standardised Southern Ocean air was analysed at regular intervals, typically every

120 minutes, and if required a drift correction was applied.
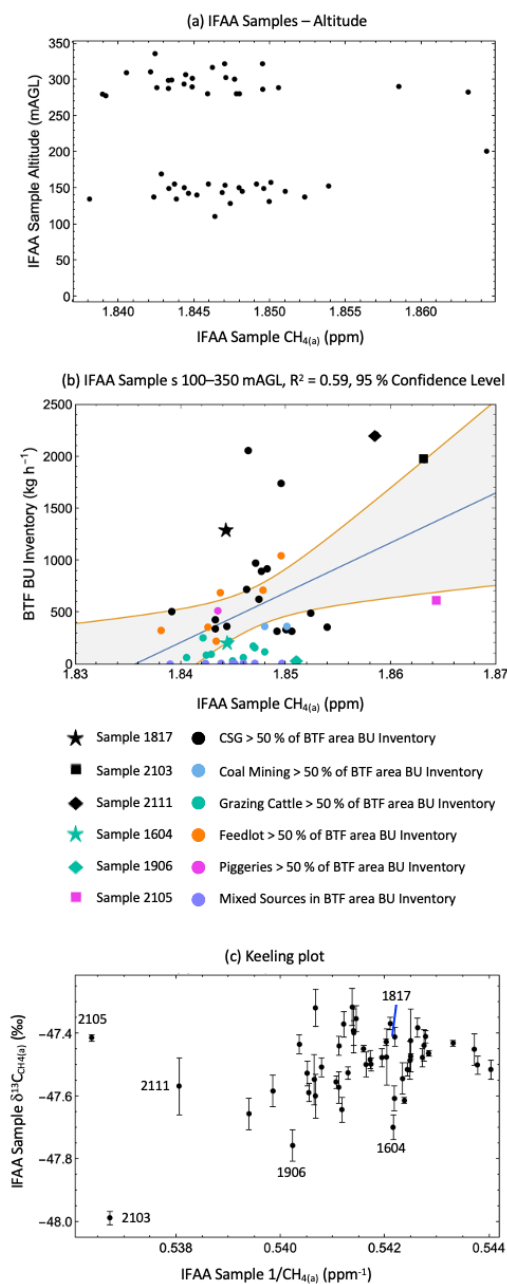
Figure 3. IFAA sample observations between altitudes 100–350 mAGL. (a) IFAA sample altitude (mAGL)) versus IFAA sample $CH_{4(a)}$

320 (ppm). (b) Back trajectory footprint bottom-up (BTF BU) inventory CH_4 (kg h^{-1}) versus IFAA sample $CH_{4(a)}$ (ppm). The linear regression

fit highlights the moderate correlation ($R^2 = 0.59$) between the two variables. (c) IFAA samples $\delta^{13}C_{CH4(a)}$ versus IFAA sample $1/CH_{4(a)}$

(ppm) (for $1/CH_{4(a)}$ the errors are too small to be observable; IFAA samples 1604, 1817, 1906, 2103, 2105 are discussed in detail in the main

text).

At RHUL, a Picarro G1301 CRDS (Picarro, Inc., USA) and a modified gas chromatography isotope ratio mass spectrometry
325 (GC-IRMS) system (Trace Gas and Isoprime mass spectrometer, Elementar UK Ltd., UK) (Fisher et al., 2006) were used for
the measurement of CH_4 mole fraction and $\delta^{13}C_{CH4}$ respectively. The Picarro G1301 CRDS has a reproducibility of $\pm$ 0.0003
ppm. Air standards from National Oceanic and Atmospheric Administration (NOAA) were used to calibrate the CRDS to the
WMO X2004A scale (Dlugokencky et al., 2005; WMO, 2020). The CH_4 mole fraction of each IFAA sample was determined
by analysing the sample for 210 seconds on the Picarro G1301, and the average value of the last 90 seconds was recorded. All
330 IFAA samples were measured in triplicate to obtain $\delta^{13}C_{CH4(a)}$ on the Vienna Pee Dee Belemnite (VPDB) scale using GC-
IRMS. When the standard deviation of the first three analyses was greater than the target instrument precision of 0.05 ‰, a
fourth analysis was performed. For more detailed information about the instrumentation and measurement procedure, see
Fisher et al. (2006) and Lu et al. (2021).

335 **2.7 Points of interest identification and application of multi-Keeling-model regression**

Different CH_4 formation processes result in each CH_4 source having different $\delta^{13}C_{CH4}$ population statistics for both the range
and distribution shape (Whiticar, 1999; Sherwood et al., 2017, 2020; Menoud et al. 2022a). Thus, the isotopic composition of
air samples can be used to identify inputs from similar sources, the extent of mixing of two or more sources, and to identify
340 samples that are offset to the isotopic composition expected from the BU inventory. IFAA samples of interest are those that
have relatively high $CH_{4(a)}$ or different than expected $\delta^{13}C_{CH4(a)}$ (for brevity called outliers) because these samples may indicate
over- or underestimation of CH_4 emissions in the BU inventory. Outliers can also indicate that a source of CH_4 has been missed
in the BU inventory. An outlier may also indicate sampling or measurement errors, but this is unlikely for the samples analysed,
due to the quality assurance measures at all stages of sampling and measurement.
345

Subsets of samples were collated based on altitude (Fig. 3 (a)) and the dominant CH_4 source in the BTF BU inventory (Table
A3). Before sorting the data into subsets, outliers were identified by visual inspection using two graphs: BTF BU Inventory vs
IFAA sample CH_4 (Fig. 3 (b)), and a Keeling plot ($\delta^{13}C_{CH4(a)}$ vs 1/$CH_{4(a)}$) (Fig. 3 (c)). Although the outliers were removed for
the Keeling model regression analysis, they are still analysed in the context of their position within the Keeling plot (Fig. 3
350 (c)). After the outliers were identified, the IFAA samples that had a single source that represented over 50 % of the 2-hour
back-trajectory inventory were combined into sets for the multi-Keeling-model regression with shared parameters analysis.
Keeling analysis sets for the following categories were collated:
- *CSG >50 % BTF BU inventory, 100–200 mAGL*
- *CSG >50 % BTF BU inventory, 250–350 mAGL*
355 - *Grazing Cattle >50 % BTF BU inventory, 100–200 mAGL*
- *Grazing Cattle >50 % BTF BU inventory, 250–350 mAGL*
- *Feedlots >50 % BTF BU inventory, 100–350 mAGL.*

For piggeries and coal mines there are only 2 BTF BU inventories with >50 % emissions from these sources (Table A3). As a
360 result, these categories could not be analysed using the modelling methods below. There is only one category for feedlots,
because there are too few points for the Keeling analysis in the 100–200 mAGL and 250–350 mAGL data sets.

For two-endmember mixing (a source of CH_4 mixed in background air), the isotopic signature of the source mixing in
background air is calculated using the Keeling model method (Keeling, 1961; Pataki et al., 2003). The Keeling model is:

365 $\delta^{13}C_{CH4(a)} = CH_{4(b)} \left(\delta^{13}C_{CH4(b)} - \delta^{13}C_{CH4(s)} \right) \cdot 1/ CH_{4(a)} + \delta^{13}C_{CH4(s)}$ \hfill (1)

where $CH_{4(a)}$ and $\delta^{13}C_{CH4(a)}$ are the IFAA sample values, $CH_{4(b)}$ and $\delta^{13}C_{CH4(b)}$ are the background air values, and $\delta^{13}C_{CH4(s)}$ is the isotopic composition of the source.

In this study, for each source category 4–10 IFAA samples were collected where a single source category contributed >50 %
370 of the BTF BU inventory emissions. For each category the samples were collected on different days and each day would have subtly different $CH_{4(b)}$ and $\delta^{13}C_{CH4(b)}$. Regression of a single source data set is poorly constrained, resulting in large uncertainties in the derived $\delta^{13}C_{CH4(s)}$ due to the low enhancement above background, less than 0.040 ppm, and the small number of samples in each category. To improve the confidence in the derived $\delta^{13}C_{CH4(s)}$, $\delta^{13}C_{CH4(b)}$ and $CH_{4(b)}$, the Keeling model (Eq. 1) was fitted simultaneously to all source category data sets using multi-Keeling-model regression with shared
375 parameters ($CH_{4(b)}$ and $\delta^{13}C_{CH4(b)}$), calculated using the MultiNonlinearModelFit function in Mathematica (Version 12.0) (Wolfram Research Inc, 2019). Comprehensive details about the Mathematica MultiNonlinearModelFit function for fitting multiple data sets to multiple expressions that share parameters is available from the Wolfram function repository (Smit, 1986).

When the multi-Keeling-model regression with shared parameters is applied to each category data set, the starting values for
380 $\delta^{13}C_{CH4(CSG-100to200)}$, $\delta^{13}C_{CH4(CSG-250to350)}$, $\delta^{13}C_{(Grazing-100to200)}$, $\delta^{13}C_{CH4(Grazing-250to350)}$ and $\delta^{13}C_{CH4(Feedlots-100to350)}$ are unconstrained (allowed to vary during the regression). Background air $CH_{4(b)}$ and $\delta^{13}C_{CH4(b)}$ are also unconstrained and a single optimal set determined. This assumes that $CH_{4(b)}$ and $\delta^{13}C_{CH4(b)}$ are similar on all days, which both the continuous ground surveying and airborne measurements results support (Lu et al. 2021; Neininger et al. 2021). This assumption is discussed further in section 3.1. Because there are subtle changes in $CH_{4(b)}$ and $\delta^{13}C_{CH4(b)}$ throughout the campaign the multi-Keeling-model regression
385 determined values for $CH_{4(b)}$ and $\delta^{13}C_{CH4(b)}$ represent the background air centroid for all days of measurements.

Miller and Tans (2003) discussed rearranging Eq. 1 for different data collection scenarios and regression aims. One algebraic expression rearrangement enables the source signature to be determined when $CH_{4(b)}$ and $\delta^{13}C_{CH4(b)}$ are unknown:

$$\delta^{13}C_{CH4(a)}\,CH_{4(a)} = \delta^{13}C_{CH4(s)}\,CH_{4(a)} + CH_{4(b)}\,(\delta^{13}C_{CH4(b)} - \delta^{13}C_{CH4(s)}). \qquad (2)$$

390 Like Eq. 1, when Eq. 2 is fitted to individual categories it is poorly constrained for the dimensions of the data sets analysed.

A second algebraic expression rearrangement by Miller and Tans (2003) requires $\delta^{13}C_{CH4(b)}$ and $CH_{4(b)}$ to be specified:

$$\delta^{13}C_{CH4(a)}\,CH_{4(a)} - \delta^{13}C_{CH4(b)}\,CH_{4(b)} = \delta^{13}C_{CH4(s)}\,(CH_{4(a)} - CH_{4(b)}). \qquad (3)$$

For Eq. 3 $CH_{4(b)}$ and $\delta^{13}C_{CH4(b)}$ can be either constant or varying in time. A multi-Miller-Tans model regression is equivalent to assuming constant $CH_{4(b)}$ and $\delta^{13}C_{CH4(b)}$, and under this assumption fitting either Eq. 1 or Eq. 3 using multiple regression
395 with shared $CH_{4(b)}$ and $\delta^{13}C_{CH4(b)}$ will result in the same values being determined for the shared $CH_{4(b)}$ and $\delta^{13}C_{CH4(b)}$. Similarly, for each category almost identical values for $CH_{4(b)}$ and $\delta^{13}C_{CH4(b)}$ are determined within the precision of the simultaneous multiple regression calculations.

In Lu et al. (2021) Bayesian regression was used, and the credible interval (CrI) reported. The frequentist 95 % confidence
400 interval (CI) is analogous to the Bayesian CrI (Lu et al. 2012; Albers et al. 2018). To allow direct comparison between this study and Lu et al. (2021) the 95 % confidence interval is reported below for $\delta^{13}C_{CH4(s)}$. Focusing on the model fit within the $1/CH_{4(a)}$ IFAA sample interval range, a useful measure for this study is to examine the single prediction confidence interval, and these values are also reported below.

405 A subset of visually identified outliers is analysed using the results of the multi-Keeling-model regression. Using the values for $CH4_{(b)}$ and $\delta^{13}C_{CH4(b)}$ derived from the multi-Keeling-model regression, the Keeling model (Eq. 1) is fitted to an outlier

subset with low $\delta^{13}C_{CH4(a)}$ values to determine $\delta^{13}C_{CH4(s)}$ for the outlier subset. For this subset a similar result could be obtained using Eq. 2.

410 **3 Results**

3.1 Background air CH$_{4(b)}$ and $\delta^{13}C_{CH4(b)}$ insights

In a region with so many sources (Figs. 1 and 2), collecting IFAA samples to define both background CH$_{4(b)}$ and $\delta^{13}C_{CH4(b)}$ was not successful. Each day IFAA samples were collected remote from sources (Fig. 1 (a)) with the aim of providing data to define background CH$_{4(b)}$ and $\delta^{13}C_{CH4(b)}$. Subsequent analysis of all the IFAA samples indicated that none of the IFAA samples 415 matched the low CH$_4$ mole fractions recorded in Neininger et al. (2021). Here, we provide further information as context for background CH$_{4(b)}$ and $\delta^{13}C_{CH4(b)}$ for comparison with the Keeling model results. The background CH$_4$ mole fraction recorded in continuous airborne surveys in Neininger et al. (2021) was stable between days and varied between 1.822 ppm and 1.827 ppm. This range was established over two weeks with varying wind directions. For the period analysed in this study the wind directions were from: 16th, southwest averaging 8.6 m s^{-1}; 18th, north averaging 4.1 m s^{-1}; 19th, northwest averaging 6.8 m s^{-1}; 420 and 21st, southeast averaging 5.4 m s^{-1}. How the background CH$_4$ mole fraction was defined each day is discussed at length in the supporting information of Neininger et al. (2021).

There is no official atmospheric greenhouse gas monitoring station in the Surat Basin, or anywhere in Queensland. The closest monitoring station is at Cape Grim, 1,500 km south, which for September 2018 recorded averages of 1.8300 ppm and −47.3 425 ‰ (https://capegrim.csiro.au/).

3.1 IFAA sample locations and CH$_4$ enhancement relationships

In Fig. 1 the location of the IFAA samples is shown. Most of the samples were collected near or above the CSG fields. As part 430 of the surveying on both the 16th and 18th, IFAA samples were collected remote from CSG production above the agricultural districts. Fig. 3 (a) shows that the IFAA samples were collected at two focused-altitude intervals, between 100 mAGL and 200 mAGL, with most IFAA samples collected at approximately 150 mAGL, and between 250 mAGL and 350 mAGL, with most samples collected at approximately 300 mAGL.

435 A plot of the BTF BU inventory emissions (kg h^{-1}) versus IFAA sample CH$_4$ (ppm) shows that there is a moderate correlation ($R^2 = 0.59$) (Fig. 3 (b)). This moderate correlation is expected because the inventory is calculated using annual data, and the rate of emissions for many CH$_4$ sources in the inventory will vary either throughout the seasons (agriculture) or daily (for example, CSG production or grazing cattle location). In Fig. 3 (b) three samples have relatively high CH$_4$ values (IFAA samples 2103, 2105, and 2111) and these points are discussed in detail below. IFAA samples 1604, 1817, and 1906 are also 440 highlighted for later discussion.

The IFAA samples are shown in a Keeling plot (Fig. 3 (c)). In this graph three points with relatively low $\delta^{13}C_{CH4(a)}$ measurements are highlighted: 1604, 1906 and 2103. These three points were not included in the initial Keeling analysis but are analysed using insights from the multi-Keeling-model regression.

445

3.2 IFAA samples $\delta^{13}C_{CH4(a)}$ versus BTF BU inventory source category contribution

The back trajectories calculated using HYSPLIT for each day are shown in Fig. A1. The trajectories shown in Figs. A1, A3, A4 and A5 are for three hours, but the footprint calculations used only the 2-hour trajectory distance (Fig. A2). The total

emissions from each IFAA sample's HYSPLIT BTF were determined based on the UNSW BU inventory (Neininger et al.

450 2021, supplementary material document) and listed in column 8, Table A3. The total CH$_4$ emissions in each IFAA sample's BTF range from 2.7 kg h^{-1} to 2209.1 kg h^{-1} (each BTF BU inventory is a subset of the UNSW inventory). Five source categories account for most of the CH$_4$ emissions in the Surat Basin: CSG, feedlots, grazing cattle, piggeries, and coal mine emissions (Neininger et al., 2021). The contribution of the individual source categories to the total emissions in the BTF were calculated as outlined in Neininger et al., (2021) and are expressed as percentages of the total emissions in Fig. 4.

455
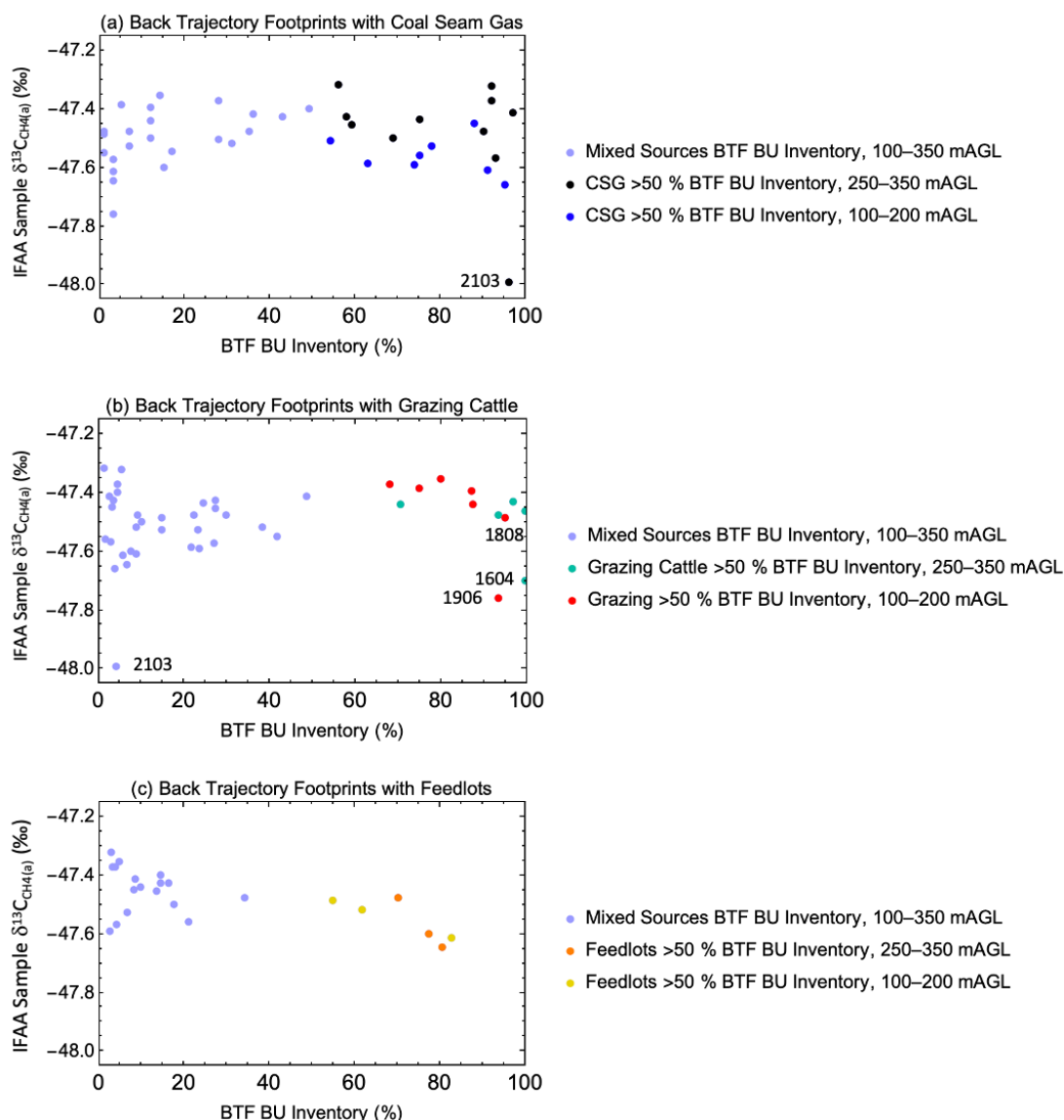
Figure 4. IFAA sample δ^{13}C$_{CH4(a)}$ (‰) versus percentage of BTF BU inventory emissions of the source categories indicated in the figure titles (%). a) BTF BU inventories with CSG CH$_4$ contributions; outlier 2103 was excluded from the Keeling modelling set. b) BTF BU inventories with grazing cattle CH$_4$ contributions; outliers 1604, 1906 and 2103 were excluded from the Keeling modelling sets. IFAA

460 sample 1808 was also excluded. (c) BTF BU inventories with feedlot CH$_4$ contributions. Category sets used in the Keeling plot modelling are each indicated by a separate colour, as shown in the colour keys. Samples below the 50 % BTF BU inventory threshold were excluded from the Keeling modelling.

There are three unknown parameters in the Keeling model (Eq. 1) ($\delta^{13}C_{CH4(s)}$, $CH_{4(b)}$ and $\delta^{13}C_{CH4(b)}$) and one independent variable (CH_4 (x-axis $1/CH_4$ in the Keeling plot)). To fit the Keeling model (Eq. 1) using the NonLinearModelFit and
465   MultiNonLinearModelFit functions in Mathematica, a minimum of four IFAA samples is required (four $CH_{4(a)}$ and $\delta^{13}C_{CH4(a)}$ pairs).

For inclusion in the Keeling analysis input set for each CH_4 source category, an individual source (CSG, grazing cattle or feedlots) had to contribute >50 % of the BTF CH_4 emissions (Table A3). The 50 % threshold was set to have enough points in
470   each Keeling modelling set, and still have one source potentially dominate the emissions. For each source category the set of samples that matched the threshold criteria is highlighted in colour in Fig. 4 and Table A3. IFAA samples excluded from the initial Keeling analysis are labelled in Figs. 4 (a) and 4 (b). The exclusion of sample number 1808 from the *Grazing >50 % BTF BU inventory, 100–200 mAGL* set is discussed below. The HYSPLIT back trajectories for each IFAA sample are shown in Figs. A3, A4 and A5. These trajectories highlight that neither a single point source nor plume was sampled. Rather multiple
475   plumes, where one source category dominated emissions, were analysed as a set (Fig. 4).

3.3 Multi-Keeling-model regression using shared parameters

480   In Fig. 5 (a) the result of using multi-Keeling-model regression with shared background $CH_{4(b)}$ and $\delta^{13}C_{CH4(b)}$ is shown, and the regression statistics are summarised in Table A4. Because $CH_{4(b)}$ and $\delta^{13}C_{CH4(b)}$ are shared parameters all Keeling lines converge to a common point for background air. The resulting values of this regression for the mole fraction and isotopic composition of the background are $CH_{4(b)}$ = 1.825 ppm (CI 95 % ± 0.037 ppm) and $\delta^{13}C_{CH4(b)}$ = −47.3 ‰ (CI 95 % ± 0.3 ‰). The resulting $\delta^{13}C_{CH4(s)}$ signatures for each category from the application of multi-Keeling-model regression with shared $CH_{4(b)}$
485   and $\delta^{13}C_{CH4(b)}$ are: *CSG >50 % BTF BU inventory, 100–200 mAGL* −65.3 ‰ (CI 95 % ± 13.1 ‰); *CSG >50 % BTF BU inventory, 250–350 mAGL*, −55.5 ‰ (CI 95 % ± 13.4 ‰); *Grazing Cattle >50 % BTF BU inventory, 100–200 mAGL*, −52.5 ‰ (CI 95 % ± 18.8 ‰); *Grazing Cattle >50 % BTF BU inventory, 250–350 mAGL*, −60.5 ‰ (CI 95 % ± 15.2 ‰); and *Feedlots >50 % BTF BU inventory, 100–350 mAGL*, −69.5 ‰ (CI 95 % ± 22.1 ‰). The single prediction confidence intervals are listed in Table A5, and for all categories they are ± 0.1 ‰.

490

In Fig. 5(b) the result of using multi-Miller-Tans model regression with shared background $CH_{4(b)}$ and $\delta^{13}C_{CH4(b)}$ is shown, and the regression statistics are summarised in Table A4. As expected, these are within measurement error identical to the Keeling model results. For this reason, the results below are discussed with reference only to the Keeling model algebraic expression representation of the two-endmember mixing model. For the reader interested in seeing the results of fitting the Keeling (Eq.
495   1) and Miller Tans (Eq. 2) models to the individual categories they are presented in Appendix B.

4 Discussion

In this study we applied multi-Keeling-model regression with shared $CH_{4(b)}$ and $\delta^{13}C_{CH4(b)}$, to determine the centroid values throughout the campaign for $CH_{4(b)}$ and $\delta^{13}C_{CH4(b)}$, and the $\delta^{13}C_{CH4(s)}$ value for each category set. The isotopic source signatures established using this approach are then compared against the values obtained from the ground observations for the major CH_4
500   sources established in Lu et al. (2021) (Table A2). Below we also discuss the extent of agreement between the 2-hour upwind BU inventory versus the expected value based on the BU inventory (Table A3). For the IFAA samples discussed below details about the sample location, day and time of collection, and the upwind inventory are listed in Table A2. For CSG and grazing cattle the higher altitude results are discussed first because these subsets had excellent agreement with the ground observations in Lu et al. (2021).
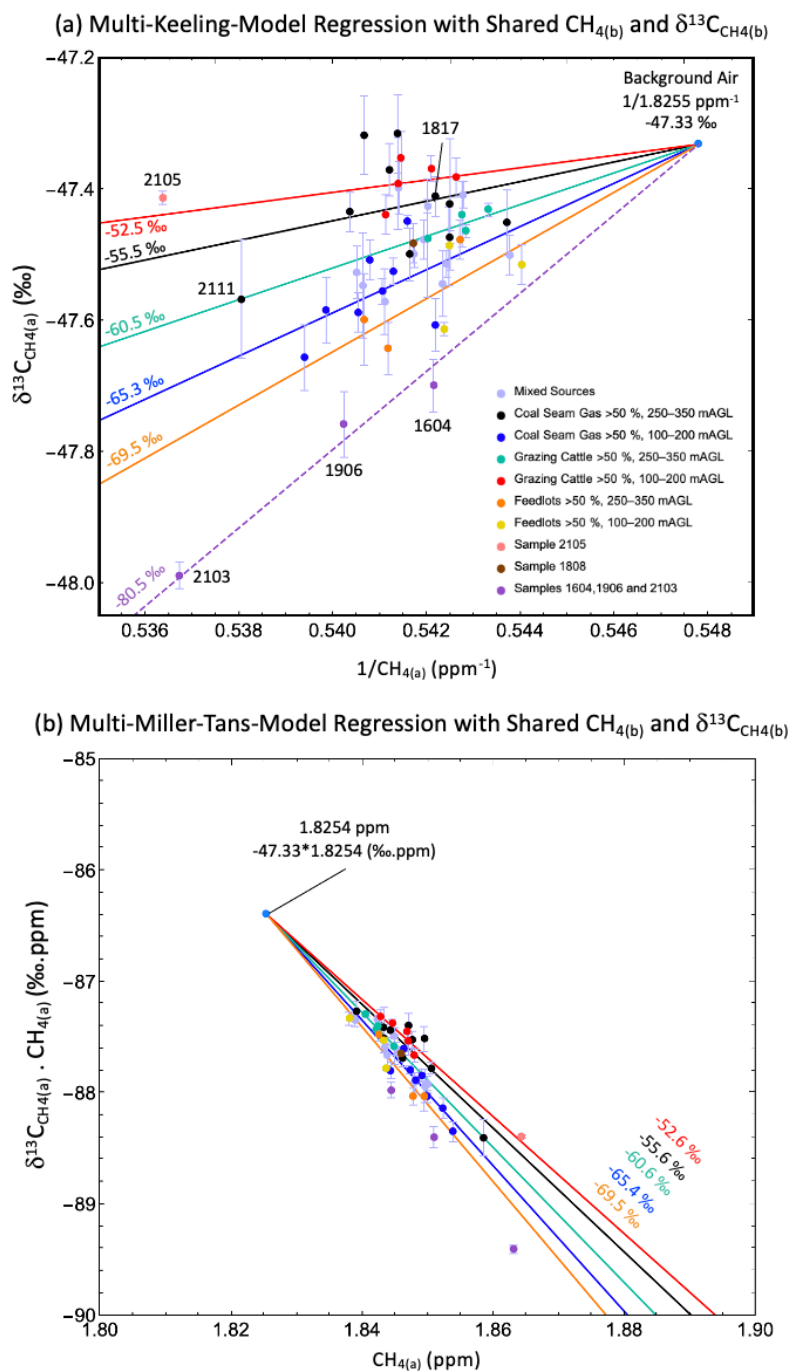
Figure 5. Multiple regression with shared $CH_{4(b)}$ and $\delta^{13}C_{CH4(b)}$ for the Keeling model ((a), solid lines, Eq. 1) and the Miller-Tans model ((b), solid lines, Eq. 3) for the category subsets listed in the colour key. Refer to Tables A4 and A5 for all regression results and their error statistics. The isotopic signature for each category, $\delta^{13}C_{CH4(s)}$, is listed near the lines of best fit for each category. The dashed purple line in (a) shows a Keeling model (Eq. 1) fitted to IFAA samples 1604, 1906, and 2103 (for this regression $CH_{4(b)}$ and $\delta^{13}C_{CH4(b)}$ were fixed to match the results of the multi-Keeling-model regression with shared $CH_{4(b)}$ and $\delta^{13}C_{CH4(b)}$). To highlight the subtle differences in the multiple regression best fit parameters, the derived $CH_{4(b)}$ and $\delta^{13}C_{CH4(b)}$ values are given to an extra significant figure in (a) and (b) compared to the measurement precision.

505

510

4.1 Source category Keeling analysis results

4.1.1 Background

During the multi-Keeling-model regression calculation, the values for $CH_{4(b)}$ and $\delta^{13}C_{CH4(b)}$ were allowed to vary. The resulting values of for the mole fraction and isotopic composition of the background are $CH_{4(b)}$ = 1.825 ppm (CI 95 % ± 0.037 ppm) and $\delta^{13}C_{CH4(b)}$ = −47.3 ‰ (CI 95 % ± 0.3 ‰). This result falls within the $CH_{4(b)}$ range reported in Neininger et al. (2021) (between 1.822 ppm and 1.827 ppm), and $\delta^{13}C_{CH4(b)}$ matches the Cape Grim value for the corresponding month (−47.3 ‰). The good match of the regression-derived $CH_{4(b)}$ and $\delta^{13}C_{CH4(b)}$ with the independent measurements of $CH_{4(b)}$ and $\delta^{13}C_{CH4(b)}$ demonstrates that multi-Keeling-model regression is a useful methodology for obtaining insights about the isotopic composition of the atmosphere.

4.1.2 CSG >50 % BTF BU inventory, 250–350 mAGL

IFAA samples included in this set were collected on all days (16th, 18th, 19th and 21st, September 2018) and under different prevailing wind directions (Fig. A3 (a)). These samples were collected either directly over or immediately adjacent to the CSG fields and the resulting $\delta^{13}C_{CH4(s)}$ signature can be considered representative for blended CSG CH_4 sources. The IFAA sample-derived isotopic signature for *CSG >50 % BTF inventory, 250–350 mAGL*, was −55.5 ‰ (CI 95 % ± 13.4 ‰), which is within the range listed in Table A2 (CrI: −56.7 ‰ to −45.6 ‰) for CSG sources measured in Lu et al. (2021). The large uncertainties are due to the small CH_4 enhancement, the small number of samples in each category data set, and the fact that in most cases there will be some small measure of input from multiple endmembers, although everything is modelled as if there is two endmember mixing (one source and background air). The overlap between the calculated and expected $\delta^{13}C_{CH4(s)}$ is shown graphically in Fig. 6 (a). Fig. 4 (a) shows that 5 of the 10 sample points had greater than 90 % of the emissions in the BTF BU inventory derived from CSG sources, and in each case most of the CH_4 emissions were from CSG compression stations. This result further validates both the methodology used in this study and the results in Lu et al. (2021).
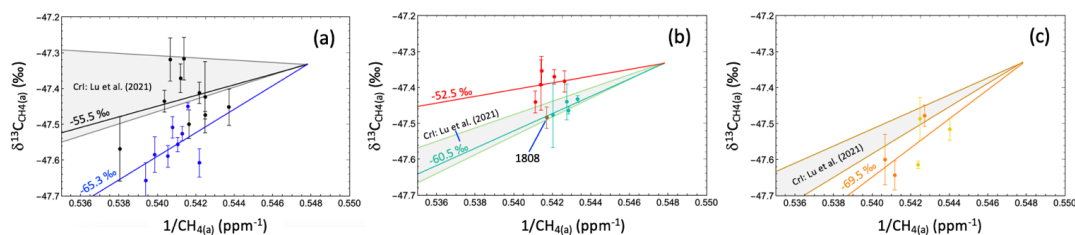
Figure 6. Expected versus measured $\delta^{13}C_{CH4(a)}$ for each CH_4 source category. The expected source category $\delta^{13}C_{CH4(s)}$ values from Lu et al. (2021), Table A2, are shown as thin continuous Keeling lines (without number values) for the upper and lower Bayesian credible interval for the category (where the credible interval is analogous to the 95 % confidence interval). The thick lines represent Keeling lines based on the IFAA samples (including derived source signatures. The IFAA sample point and measurement uncertainty are also shown for each category data set. The categories are: (a) *CSG >50 % BTF inventory, 100–200 mAGL* (blue) and *CSG >50 % BTF inventory, 250–350 mAGL* (black); (b) *Grazing Cattle >50 % BTF inventory, 100–200 mAGL* (red) and *Grazing Cattle >50 % BTF inventory, 250–350 mAGL* (green); (c) *Feedlots >50 % BTF inventory, 100–350 mAGL* (yellow points (100–200 mAGL) and orange points (250–350 mAGL)).

4.1.3 CSG >50 % BTF BU inventory, 100–200 mAGL

555   For the *CSG >50 % BTF BU inventory, 100–200 mAGL* set the isotopic signature was −65.3 ‰ (CI 95 % ± 13.2 ‰) (Figs 4 (a) and 6 (a)). This is considerably isotopically lighter than the higher-altitude CSG set discussed above and lower in value compared to all previous CSG measurements from Lu et al. (2021). The 100–200 mAGL CSG $\delta^{13}C_{CH4(s)}$ signature is within the $\delta^{13}C_{CH4(s)}$ signature range reported in the literature for the Walloon Coal Measures, −64.1 ‰ to −44.5 ‰ (Baublys et al., 2015; Draper and Boreham, 2006; Hamilton et al., 2014, 2015; Iverach et al. 2015, 2017; Stalker and Smith, 2004), but is

560   isotopically lighter than the range reported in Lu et al. (2021). In Fig. 6 (a) all 100–200 mAGL samples are systematically isotopically lighter than the high altitude 250–350 mAGL IFAA samples. This offset is difficult to explain from the data collected.

   With reference to the results in Table A3, the lower 100–200 mAGL CSG set had no significant difference in the median CH_4

565   compared to the higher 250–350 mAGL set (1.849 ppm to 1.847 ppm, respectively). However, there are two noticeable differences between the high and low altitude CSG sets: the median BTF BU inventory emission rate is 380 kg h^{-1} lower for the 100–200 mAGL altitude set; and CSG sources for the 100–200 mAGL set tally to a median emission rate that is 187 kg h^{-1} less than the 250–350 mAGL CSG set. But these differences do not account for the lighter $\delta^{13}C_{CH4(s)}$ signature for the 100–200 mAGL CSG set. There was also no significant difference between the low and high CSG BTF BU inventories with respect

570   to either the grazing cattle or feedlot percentage inputs. Both CSG sets have samples collected on the 18th, 19th and 21st; both sets cover a range of CSG areas (Fig A3). In Fig 6 (a) all these lower altitude samples where the upwind inventory is dominated by CSG sources are isotopically lighter than expected.

   For three samples in the 100–200 mAGL CSG set (1821, 1823 and 1911), greater than 88 % of the BU inventory emissions

575   are due to CSG sources (Table A3), thus a $\delta^{13}C_{CH4(s)}$ value of -56.7 ‰ to -45.6 ‰ would be expected (Table A2). However, these samples are part of a category set that had a best fit value of -65.3 ‰. Assuming that there are no major issues with the inventory, it would suggest that the ground-based study (Lu et al. 2021) did not capture the full $\delta^{13}C_{CH4(s)}$ population range for CSG sources. The low -65.3 ‰ value could also be explained by a higher proportional contribution from cattle emissions on the day of sampling, or unaccounted emissions from termites. Ideally future chemical analysis of airborne collected air samples

580   should include the measurement of δD to assist with constraining source attribution.

4.1.4 Grazing Cattle >50 % BTF BU inventory, 250–350 mAGL

   There were only four 250–350 mAGL IFAA samples where grazing cattle contributed >50 % of the BTF BU inventory

585   emissions. These four points were clear of most other sources of emissions (Fig A4 (a)). The prevailing wind was from the southwest for sample 1603, and from the northeast for samples 1803, 1804, and 1805. Prior to sample collection the air had travelled over regions dominated by agriculture, mostly grazing cattle and mixed cropping. The multi-Keeling-model regression $\delta^{13}C_{CH4(s)}$ signature for the category *Grazing Cattle >50 % BTF BU inventory, 250–350 mAGL* was −60.5 ‰ (CI 95 % ± 15.2 ‰) (Fig 6 (b)). This matches the grazing cattle result in Lu et al. (2021). This result indicates that in mixed

590   cropping districts where grazing cattle are the dominant source of CH_4 emissions, the expected and measured $\delta^{13}C_{CH4(a)}$ align.

4.1.5 Grazing Cattle >50 % BTF BU inventory, 100–200 mAGL

   IFAA sample 1808 meets the initial criteria for the *Grazing Cattle >50 % BTF BU inventory, 100–200 mAGL* set but it was

595   excluded from the set used in the Keeling analyses for the following three reasons. Sample 1808 was collected on a different

day compared to the other samples in this set (1903, 1904, 1908, 1910 and 1912); it was collected above a region dominated by agriculture and in Fig. 6 (b) the sample falls on the grazing cattle $\delta^{13}C_{CH4(s)}$ signature Keeling line established for the *Grazing Cattle >50 % BTF BU inventory, 250–350 mAGL* set.

600 The multi-Keeling-model regression $\delta^{13}C_{CH4(s)}$ signature for the category *Grazing Cattle >50 % BTF BU inventory, 100–200 mAGL*, using only the samples collected on the 19th, was −52.5 ‰ (CI 95 % ± 18.8 ‰). This is too isotopically heavy for cattle and is closer to the expected value for CH_4 emissions from CSG (Figs. 5 (b) and 6 (b)). The prevailing winds for samples 1903, 1904, 1908, and 1910 were from the northwest. Just beyond the 3-hour back trajectories shown in Fig. A4 (b) the air parcels would have travelled over the largest northwest Surat Basin gas fields near Woleebee Creek, which contains CSG plants,
605 distribution hubs, and water treatment facilities. It is highly likely that CH_4 emissions from the north-western Surat Basin CSG facilities have been sampled in the north of the study area on 19th Sept 2018.

4.1.6 Feedlots >50 % BTF inventory, 100–350 mAGL

610 Due to too few points meeting the threshold requirement for the 100–200 mAGL and 250–350 mAGL categories the feedlot set was obtained by combining both altitude sets. The derived multi-Keeling-model regression $\delta^{13}C_{CH4(s)}$ signature for the category *Feedlots >50 % BTF inventory, 100–350 mAGL* was −69.5 ‰ (CI 95 % ± 22.1 ‰), which is isotopically lighter than the −65.2 ‰ to −60.3 ‰ (CrI) listed for feedlots in Table A3 and shown in Fig. 6 (c), but still compatible within the derived 95% confidence intervals. There are also too few values in the literature to fully characterise the population statistics for the
615 $\delta^{13}C_{CH4(s)}$ signature of feedlot emissions in Australia, and this result may be simply better characterising the $\delta^{13}C_{CH4(s)}$ signature population range for feedlots. Another option to be explored as part of further ground studies is that there may be other isotopically lighter biological sources associated with the feedlots. For example, one of the feedlots sampled was Australia's largest feedlot (Grassdale), which has commercial scale fertiliser production onsite (https://www.grassdalefert.com.au/), and this potential source of CH_4 is not incorporated into any of the BU inventories for the region. This may be a biological source
620 of CH_4 with a lighter isotopic signature.

4.2 Analysis of the isotopically light IFAA samples

IFAA samples 1604, 1906 and 2103 were identified as being isotopically lighter compared to the other samples and were not
625 used in any of the source category data sets. Using the multi-Keeling-model regression derived background air values (1.825 ppm and –47.3‰) the Keeling model was fitted to 1604, 1906 and 2103 (Fig 5(b) purple dashed Keeling line). The fitted model has an isotopic signature of −80.5 ‰ (CI 95 % ± 9.2 ‰). The only source listed in Table A2 that has this isotopic signature is Kangaroos, but this would not be a significant CH_4 source for these samples. There is another biological source of CH_4 that could contribute in the grazing cattle and mixed cropping districts, upwind of IFAA samples 1604 and 1906. There
630 are three sources of CH_4 listed in Sherwood et al. (2017, 2020) and Menoud et al. (2022) with $\delta^{13}C_{CH4(s)}$ signatures of −80 ‰: wetlands, waste, and termites. Of these three sources termites is the most likely, as termite mounds were observed during the field campaign in many of the forested and dryland farming regions. For IFAA sample 2103 both the brine water ponds and termites could be the missing biological source with a low $\delta^{13}C_{CH4(s)}$ signature. However, the relatively high CH_4 measured for this sample (Figs. 3 and 5) suggests that the brine ponds, or another CSG source, is likely. Below these isotopically light
635 samples are discussed in detail with reference to satellite imagery.

4.3 Keeling Plot Points of Interest

640 In Figs 3 and 4 both outliers and points of interest were identified. These points provide unique insights into overlooked sources of CH_4 in the inventory and guide where further measurements are required.

IFAA sample 1604 was collected on the western margin of the CSG field (Fig. 7). It was initially anticipated to provide a background air reference sample, but the $\delta^{13}C_{CH4(a)}$ of the air sample is −47.7 ‰, which is isotopically too light for fresh air in

645 the Surat Basin. This sample sits on a Keeling regression line with a $\delta^{13}C_{CH4(s)}$ of −80.5 ‰. From our current knowledge of the region this cannot be assigned to a source. The back trajectory passes over regions of mixed cropping and cattle, and −80.5 ‰ is 20 ‰ lighter than expected for cattle in the region. There is a cluster of piggeries with a holding capacity of 10,000 just outside the near distance BTF and another piggery cluster with a holding capacity of up to 25,000 pigs immediately upwind of the 2-hour BTF. However, the one reported $\delta^{13}C_{CH4(s)}$ signature for piggeries in Lu et al. (2021) had a value of −47.6 ‰, so

650 piggeries are highly unlikely to be the source. There are also a few CSG production wells in the area, but this source of CH_4 is isotopically too heavy. A potential source that could explain the −80.5 ‰ signature in this farming district is termites.
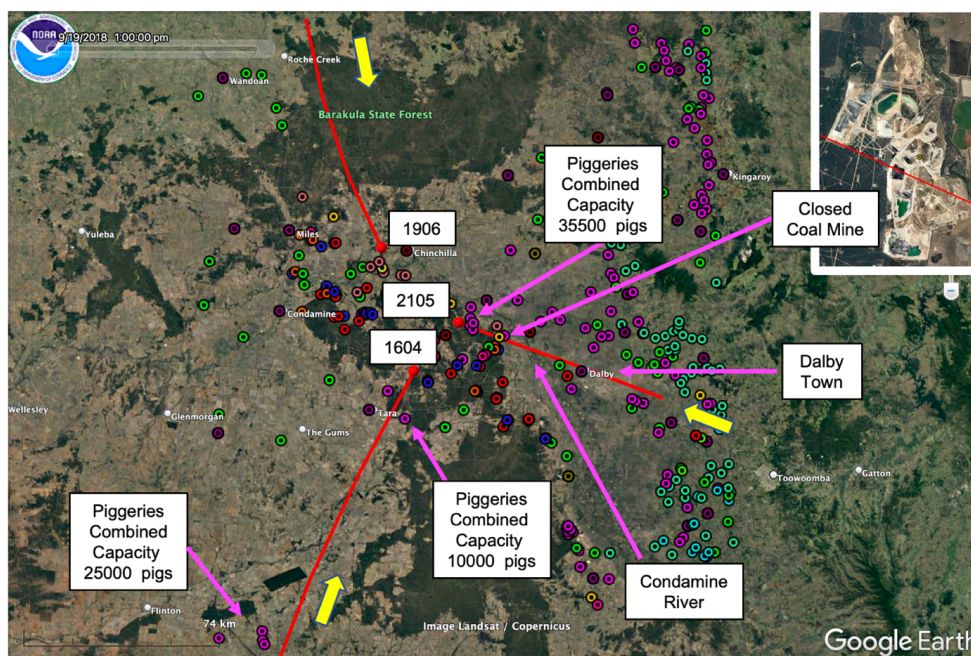
Figure 7. Three-hour back-trajectory path lines (red) for IFAA samples 1604, 1906 and 2105. Refer to Fig. A1 for the point source colour
655 key (image © Google Earth).

The two IFAA samples with the highest CH_4 mole fraction readings were downwind of the major CSG facilities (samples 2011 and 2103, Fig. 4 and Fig. 7). Sample 2103 is of particular interest because it has the lowest $\delta^{13}C_{CH4(a)}$ of any sample collected and it plots on the −80.5 ‰ Keeling line in Fig. 5 (b). The wind was moving from south-east to north-west when

660 samples 2103 and 2111 were collected about 20 km west-north-west of the Kenya water management ponds (Fig. 8). The back-trajectory centre line for sample 2111 passes directly over the Berwyndale South / Windbri central processing plant and Talinga plant (Fig. 8 (b)), and immediately to the north of the Kenya water management ponds (Fig. 8 (c)). Sample 2111 is a blended input from all these facilities. CSG sources contributed 93 % towards the CH_4 emissions in the BTF BU inventory: CSG wells 245 kg h^{-1}, CSG raw water ponds 787 kg h^{-1}, CSG compressor stations 811 kg h^{-1}, and CSG plants 210 kg h^{-1}

665 (Table A3). Feedlot cattle contributed 4 %, 88 kg h^{-1}, and grazing cattle 3 %, 64 kg h^{-1}.
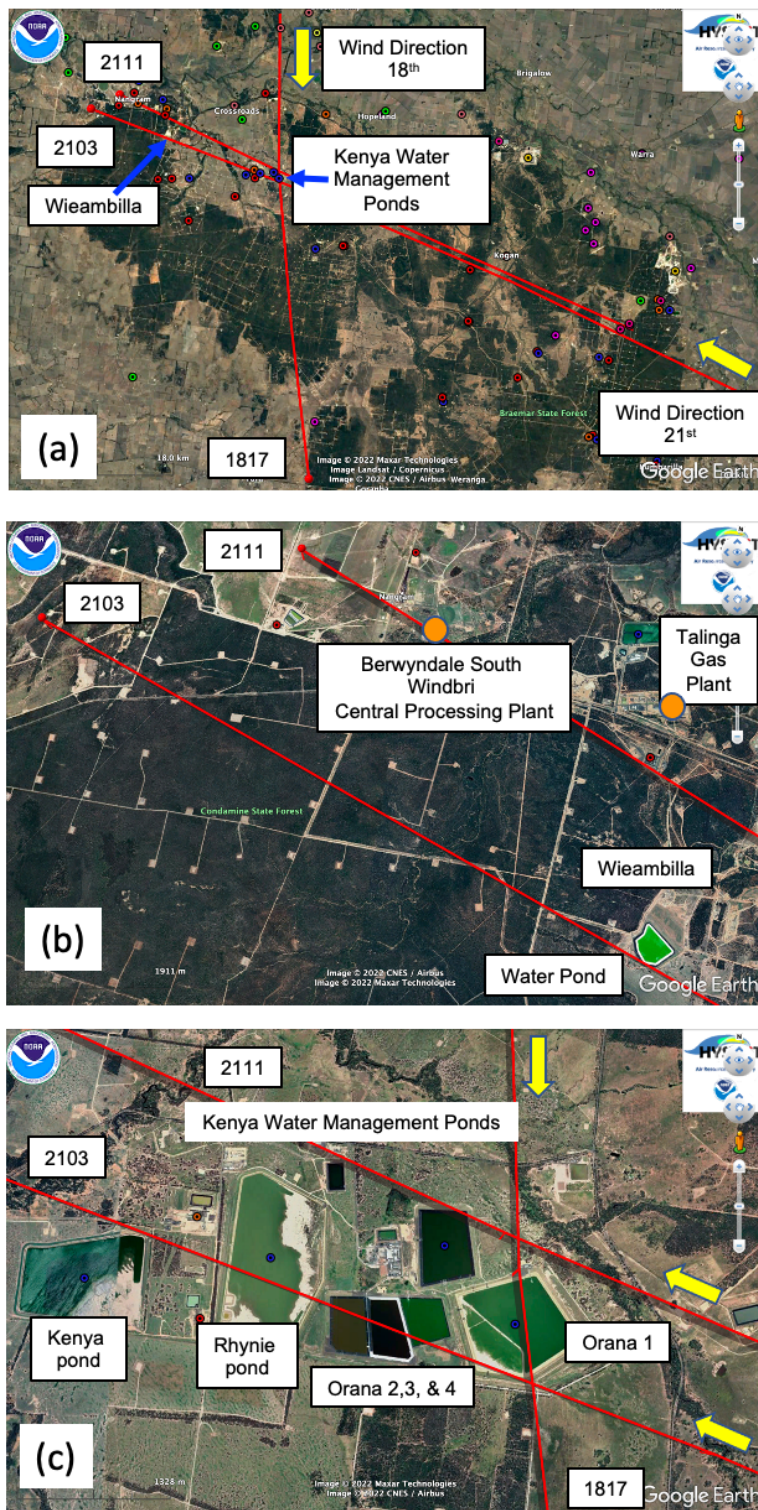
Figure 8. a) Three-hour back-trajectory path lines for IFAA samples 1817, 2103, and 2111. b) Back-trajectory paths for 2103 and 2111 relative to the Berwyndale South / Windbri Central Processing Plant and the Talinga processing plant. c) Kenya water management ponds relative to 1817, 2103 and 2111 back-trajectory centre lines (image ©Google Earth).

670

The back-trajectory centre line for 2103 passes over two sets of ponds: ponds near Wieambilla in the proximal BTF and further east at the Kenya water treatment complex (Fig. 8 (a) and 8 (c)). Kenya pond holds treated water suitable for adding to the Condamine River (Fig. 7). Orana 4 holds brine produced from the filtering of the raw water before being sent to the brine concentrator. Orana 2 and 3 hold water output from the brine concentrator (QGC 2013). No plumes were sampled near this

675 complex in Lu et al. (2021), so the $\delta^{13}C_{CH4(s)}$ of any emissions from these ponds is not known. CSG sources contributed 96 % towards the emissions in the BTF BU inventory for sample 2103: CSG wells 251 kg h^{-1}, CSG raw water ponds 586 kg h^{-1}, CSG compressor stations 714 kg h^{-1}, and CSG plants 338 kg h^{-1} (Table A3).

Upwind of IFAA sample 1906 no CH$_4$ point source is recorded in the BU inventory (Fig. 7). There is a gravel quarry that has

680 a small pond (200 m by 50 m) that could be a source of CH$_4$ emissions with a biological signature. The only other known significant CH$_4$ sources in this region are natural CH$_4$ seeps and abandoned exploration well seeps (Lu et al. 2021). Many of these are coal exploration wells that intersect seams with a biological signature (Iverach et al. 2015, Lu et al. 2021), but these sources would be expected to have a $\delta^{13}C_{CH4(s)}$ signature of approximately −60 ‰, not the observed −80.5 ‰. Like sample 1604, the $\delta^{13}C_{CH4(s)}$ signature of −80.5 ‰ for sample 1906 could be explained by termites.

685

Sample 2105 (Figs 3 (b) and Fig. 8) is dominated by piggery emissions (56 %), which have a $\delta^{13}C_{CH4(s)}$ signature of −48.0 ‰ to −47.1 ‰ (CrI), with significant CSG emissions (36%) and other minor sources (Table A3). In Fig. 3 (b) this point plots in a position suggesting that the inventory has underestimated emissions (Neininger et al. 2021). In Fig. 5 (b) this point plots just above the CSG Keeling lines. A blend of piggery and CSG emissions accounts for both the relatively high CH$_{4(a)}$ and $\delta^{13}C_{CH4(a)}$.

690 A plausible explanation for this outlier is that on the day of sampling CSG emissions were higher than indicated by the BTF BU inventory. Another possibility is that the back trajectory passes over a closed open-pit coal mine. Because this coal mine is closed it is not counted in the BU inventories. Large plumes were intersected near this coal mine during the ground surveying presented in Lu et al. (2021), and emissions from this recently closed coal mine may have been captured in sample 2105. An additional possibility to be explored as part of new ground surveys are the emissions from natural seeps along the Condamine

695 River.

Sample 1817 (Figs 3 (c), 5 (b) and Fig. 8) also has a back-trajectory line that passes over the Kenya water management ponds. It was collected 35 km south of the ponds and other major CSG facilities, which accounts for its lower CH$_4$ mole fraction. The back-trajectory centre line for 1817 passes over the eastern-most Kenya water management pond, Orana 1, which is a raw

700 water pond. CH$_4$ emitted from this pond is likely to have a similar composition to the produced gas. CSG source contributed 97 % of the CH$_4$ emissions in the BTF: CSG wells 136 kg h^{-1}, CSG raw water ponds 582 kg h^{-1}, CSG compressor stations 459 kg h^{-1}, and CSG plants 78 kg h^{-1} (Table A3). There was also a minor (2.5 %) input from grazing cattle (2.5 kg h^{-1}). This sample does not plot as an outlier (Figs. 4 (a) and 5 (a)).

705 Samples 1817 and 2111 plot in the Keeling plot (Fig. 5 (b)) in positions consistent with our knowledge of the isotopic signatures of sources in the BTF BU inventory. To explain the position of sample 2103 in Fig. 5 (b) a source of CH$_4$ with a $\delta^{13}C_{CH4(s)}$ signature of approximately −80 ‰ is required. The size and position of the Kenya water management treatment complexes associated with the water treatment, the presence of brine ponds and other waste together make this facility a potential location for the missing source of CH$_4$ with an $\delta^{13}C_{CH4(s)}$ signature of approximately −80 ‰. The back trajectory also passes over

710 forested areas where there are termites. Further fieldwork is required to answer why sample 2103 indicates a missing biological source of CH$_4$ in the inventories.

5 Summary

An objective of this study was to use IFAA samples to characterise the $\delta^{13}C_{CH4}$ source signature of emissions from facilities

715   that could not be sampled during the ground campaign (Lu et al. 2021), especially the CSG regions that are remote from public roads. This study analysed the IFAA samples using novel methods. With careful sample quality control and data sorting we have demonstrated that it is possible to use IFAA samples collected downwind of multiple common sources (e.g., one sample per feedlot, for multiple feedlots) to determine the $\delta^{13}C_{CH4(s)}$ signature for a single source category. Having access to a high-resolution BU inventory is critical for the interpretation of the IFAA $CH_{4(a)}$ and $\delta^{13}C_{CH4(a)}$ values. This inventory is required to

720   sort the data into sets based on the dominant upwind source of CH_4.

A concern after the measurements of the IFAA samples in the laboratory was that the lack of CH_4 enhancement above $CH_{4(b)}$ (less than 0.04 ppm) would not allow for the interpretation of these data using the Keeling plot method. Establishing $CH_{4(b)}$ and $\delta^{13}C_{CH4(b)}$, as traditionally done from the collated data sets, was not possible by fitting the Keeling model (Eq. 1) or the

725   Miller-Tans model (Eq. 2) to individual data sets (this is demonstrated in Appendix B). We overcame this challenge by using multi-Keeling-model regression with shared $CH_{4(b)}$ and $\delta^{13}C_{CH4(b)}$. An interpretation in alignment with other ground and continuous airborne observations was possible only after applying this regression algorithm. Despite the low CH_4 enhancement of less than 0.04 ppm the derived isotopic signatures for background air $CH_{4(b)}$ = 1.825 ppm (CI 95 % ± 0.037 ppm) and $\delta^{13}C_{CH4(b)}$ = −47.3 ‰ (CI 95 % ± 0.3 ‰) match independent observations (Tables A2 and A4).

730

The derived $\delta^{13}C_{CH4(s)}$ values for the 250–350 mAGL IFAA sample sets (Figs 6 (a) and 6 (b); Tables A2 and A4) where the inventory was dominated by CSG facilities or grazing cattle were close to those determined from the ground-based analysis of plumes (Lu et al. 2021). The airborne measurement results show where the $\delta^{13}C_{CH4(s)}$ values obtained from the ground-based studies are applicable in many of the subregions within the large study domain covering 200 km by 200 km (Fig. A3 (a)). The

735   results for the 100–200 mAGL altitude IFAA samples where the inventory was dominated by CSG facilities or grazing cattle did not match expectations and were isotopically lighter than expected (Fig. 6 (a)). There are many possible explanations that cannot be resolved using currently available data. The mismatch could be due to there being more than one dominant source category in the upwind region, incomplete mixing of all sources, sources missing from the BU inventory, the applied emission factors used for source apportionment not being precise for the individual source, or the $\delta^{13}C_{CH4(s)}$ signatures from the few

740   plumes sampled as part of the ground-based studies not being representative of the complete population statistics. Collecting δD_{CH4} samples would assist in constraining the interpretation.

In Fig. 3 (c) three outliers were identified for their relatively low $\delta^{13}C_{CH4(a)}$ values: IFAA samples 1604, 1906 and 2103. The application of multi-Keeling-model regression with shared $CH_{4(b)}$ and $\delta^{13}C_{CH4(b)}$ constrained the $\delta^{13}C_{CH4(s)}$ signature for these

745   samples to be approximately –80 ‰. For all three samples, termite emissions may have been sampled. For sample 2103, the upwind CSG brine ponds, or another CSG source close to these ponds, also needs to be investigated as a potential source of CH_4 that has not been incorporated into the BU inventories. The relatively high enhancement of atmospheric methane downwind of the CSG water management ponds indicates a potentially large CH_4 source, which could be quantified in the future using a different sampling design (e.g., mass balance flight pattern) or ground-based plume studies. CSG water

750   management ponds may also represent a mitigation opportunity. Improved separation of the methane from the water at the production well head or before placing the water into the ponds would increase the resource produced and minimise fugitive CH_4 emission.

For regional studies that require the use of a BU inventory a pragmatic decision must be made about where to place the BU

755   inventory boundary. The $\delta^{13}C_{CH4(a)}$ measurements of the 100–200 mAGL IFAA sample set collected over the grazing cattle

and mixed cropping districts on 19th Sep 2018 show that CH_4 emissions from the northwest gas field were likely entering the study domain. This highlights the usefulness of isotope studies for checking assumptions about inflowing air. It was initially thought that these samples would capture clean background air. The isotope results indicated that this was not the case.

760   The measurement of $\delta^{13}C_{CH4}$ in this study has identified that termites are potentially contributing significant quantities of CH_4 to the regional CH_4 budget. Quantifying termite CH_4 emissions from both natural and agricultural landscapes may help with closing the gap between the top-down and bottom-up CH_4 emission estimates reported in Neininger et al. (2021). More generally, atmospheric measurements of greenhouse gas emissions using satellite-, aircraft- and drone-based analysers are increasingly being used for inventory verification. The results presented in this study and in Basu et al. (2022) demonstrate

765   that isotope studies are required to constrain source attribution. To further enhance our capacity to interpret atmospheric CH_4 measurements, ideally both $\delta^{13}C_{CH4}$ and δD_{CH4} should be measured (Lu et al. 2021).

The application of the multi-Keeling-model regression with shared $CH_{4(b)}$ and $\delta^{13}C_{CH4(b)}$ enables: the characterisation of the $\delta^{13}C_{CH4(s)}$ signatures for sources not accessible during ground campaigns assuming accurate source attribution in the inventory;

770   the identification of coal seam gas subregions where there is poor agreement between the IFAA sample $\delta^{13}C_{CH4(a)}$ measurement and the $\delta^{13}C_{CH4}$ value expected from BU inventory; the identification of subregions where there must be a strong source of CH_4 with a $\delta^{13}C_{CH4(s)}$ signature of approximately –80 ‰ not recorded in the BU inventories; the identification of mitigation opportunities and the detection of CSG emissions entering the study area from outside the study BU inventory domain. The isotopic analysis methods presented in this study could be applied in any setting where there are many co-located sources of

775   CH_4 and be used to identify CH_4 source knowledge gaps in national inventories.

Author Contributions

BK, BN, JH, RF and SS were responsible for project design and securing funding. BN and JH collected the air samples. XL,
SH and BK managed the infield quality assurance testing of the air samples. RF, DL, TR, CvdV and MM managed and did
the laboratory measurements of the air samples. XL ran the HYSPLIT calculations, and BK and XL developed and analysed
the bottom-up inventory. BK conceived the use of multi-Keeling regression and did the regression analyses. XL produced
Figures 1 and 2; all other figures were produced by BK. BK wrote the manuscript with the help of XL. BN, DL, EN, JF, RF,
SH, SS, and TR all contributed to the review, additional interpretation, and editing of the manuscript.

Funding

Data collection and analysis was funded under the Climate and Clean Air Coalition (CCAC) Oil and Gas Methane Science
Studies, hosted by the United Nations Environment Programme (UNEP). Funding was provided by the Environmental
Defense Fund, Oil and Gas Climate Initiative, European Commission, and CCAC. The project funds were managed by The
United Nations Environment Programme grant numbers DTIE18-EN067, DTIE19-EN0XX and DTIE19-EN633 (UNSW
grant numbers RG181430 and RG192900). UNSW contributed matching funding via in-kind support for BK. UNSW
researcher XL was partly supported by UNEP. XL was also supported in part by UNSW–China Scholarship Council (CSC).
SH was supported by a Research Training Program scholarship from the Australian Government. SS acknowledges
additional support from the Robertson Foundation. ARA and MetAir have each contributed about 50% in-kind in accordance
with the proposal to UNEP. ARA has been substantially sponsored by the Hackett Foundation in Adelaide. MM received
funding from the European Union's Horizon 2020 research and innovation programme under the Marie Sklodowska-Curie
grant agreement No 722479, project MEMO2; https://h2020-memo2.eu/.

Acknowledgements

The authors thank the MSS Science Advisory Committee, the MSS Technical Working Group as well as Christopher Konek
and Meghan Demeter their administrative assistance. The authors also thank the UNSW grant management and finance staff.
The authors are grateful for the assistance of the staff at the Australian Government, Department of Industry, Science, Energy
and Resources for their guidance on the development of the UNSW inventory. The authors appreciate the constructive feedback
from the reviewers, which helped with improving the overall quality of the paper.

Appendix A

Table A1. Abbreviations.

810 | BTF | Back-Trajectory Footprint
| BU | Bottom-Up
| CI | Confidence Interval
| Crl | Credible Interval
| CSG | Coal Seam Gas
815 | CSIRO | Commonwealth Scientific and Industrial Research Organisation
| CRDS | Cavity Ring-Down Spectrometer
| GC-IRMS | Gas Chromatography Isotope Ratio Mass Spectrometry
| HYSPLIT | Hybrid Single Particle Lagrangian Integrated Trajectory
| IFAA | In-Flight Atmospheric Air
820 | mAGL | Metres Above Ground Level
| NOAA | National Oceanic and Atmospheric Administration
| RHUL | Royal Holloway, University of London
| TD | Top-Down
| UNFCCC | United Nations Framework Convention on Climate Change
825 | UNSW | University of New South Wales
| VPDB | Vienna Pee Dee Belemnite

Table A2. Surat Basin ground-based campaign (Lu et al. 2021) and literature $\delta^{13}C_{CH4}$ values for each source category within the study area.

UNSW Sources	$\delta^{13}C_{CH4}$ (‰) (Mean ±1 σ)	Bayesian 95 % Credible Interval (‰)	$\delta^{13}C_{CH4}$ (‰) Reference
CSG wells, venting water lines, and distributed CSG sources	−54.5 ± 0.1	−54.8 to −54.8	Lu et al. (2021)
CSG water ponds	−50.9 ± 2.8 −51.9 ± 2.3	−56.6 to −45.6 −56.7 to −47.2	Lu et al. (2021)
CSG gathering and boosting stations	−53.7 ± 0.4	−54.5 to −53.0	Lu et al. (2021)
CSG processing plants	−55.6 ± 0.4	−56.4 to −54.7	Lu et al. (2021)
Coal mines	−60.0 ± 0.6	−61.1 to −58.9	Lu et al. (2021)
Ground seeps	−59.9 ± 0.3 −60.5 ± 0.2	−60.5 to −59.2 −60.9 to −60.1	Lu et al. (2021)
Condamine river seeps	−61.2 ± 1.4	−63.9 to −58.4	Lu et al. (2021)
Feedlot cattle	−62.9 ± 1.3	−65.2 to −60.3	Lu et al. (2021)
Grazing cattle	−59.7 ± 1.0	−61.7 to −57.5	Lu et al. (2021)
Dairy cattle (Assumed similar to feedlots)	−62.9 ± 1.3	−65.2 to −60.3	Lu et al. (2021)
Piggeries	−47.6 ± 0.2	−48.0 to −47.1	Lu et al. (2021)
On-farm water bodies (dams)	−51.2	Not Measured	Day et al. (2016)
Forest nodes - kangaroos	−80	Not Measured	Godwin et al. (2014)
Domestic wood heaters and native vegetation wildfire	−22.2 ± 2.8	Not Measured	Ginty (2016)
Energy – road transport and residential	−43.4 ± 3.4	Not Measured	Lu et al. (2021)
Solid waste disposal	−52.1 ± 3.6	−59.0 to −45.3	Lu et al. (2021)
Domestic wastewater	−47.6 ± 0.2	−47.9 to −47.2	Lu et al. (2021)

830

Atmospheric Chemistry and Physics — Discussions — Open Access — EGU

Table A3. In-flight atmospheric air sample location details and UNSW bottom-up inventory CH$_4$ emissions estimates within the 2-hour back-trajectory footprint.

Airborne Sample ID (Date: Bag #)	Latitude	Longitude	Local Time	Height Above Ground (m)	CH$_4$ (ppm)	δ^{13}C-CH$_4$ (‰)	Back Trajectory Footprint Sum (kg/hour)	CSG Well (kg/hour)	CSG Raw Water (kg/hour)	Compressor Station (kg/hour)	CSG Gas Plant (kg/hour)	Sum all CSG (kg/hour)	CSG (%)	Cattle Feedlot (kg/hour)	Cattle Feedlot (%)	Condamine NRM Cattle Grazing or Crops (kg/hour)	Condamine NRM Cattle Grazing or Crops (%)	Qld MDB NRM Cattle Grazing or Crops (kg/hour)	Qld MDB NRM Cattle Grazing or Crops (%)	All Grazing (kg/hour)	All Grazing (%)	Piggery (kg/hour)	Piggery (%)	Coal Mine (kg/hour)	Coal Mine (%)	All Other (kg/hour)	All Other (%)
1603	-27.082980	150.194540	11:13:07	310	1.842	-47.5	249.9	1.2	0.0	0.0	0.0	1.2	0.0	0.0	0.0	0.0	0.0	248.7	99.5	248.7	99.5	0.0	0.0	0.0	0.0	0.0	0.0
1604	-27.157190	150.629500	11:28:00	306	1.844	-47.7	204.0	0.8	0.0	0.0	0.0	0.8	0.0	0.0	0.0	0.0	0.0	202.9	99.5	202.9	99.5	0.0	0.0	0.0	0.0	0.3	0.2
1605	-27.195490	150.858810	11:35:42	277	1.839	-47.5	505.3	24.8	0.0	125.8	148.5	299.1	59.0	67.5	13.4	0.0	0.0	137.4	27.2	137.4	27.2	0.0	0.0	0.0	0.0	1.3	0.3
1607	-27.272720	151.303290	11:50:15	321	1.850	-47.6	1041.4	73.3	46.0	0.0	34.7	154.0	15.0	803.7	77.2	6.5	0.6	72.0	6.9	78.5	7.5	0.0	0.0	0.0	0.0	5.2	0.5
1608	-27.290710	151.399020	11:53:18	288	1.843	-47.5	354.9	25.2	0.0	0.0	0.0	25.2	7.0	249.1	70.2	0.0	0.0	39.3	11.1	78.5	22.1	0.0	0.0	0.0	0.0	2.0	0.6
1611	-26.669657	151.200226	14:00:18	301	1.845	-47.4	1176.4	140.3	22.4	202.2	128.3	511.1	43.0	192.9	16.4	19.6	1.7	19.6	1.7	39.3	3.3	408.2	34.7	0.0	0.0	24.9	2.1
1617	-26.958687	151.393040	15:34:41	316	1.846	-47.5	717.4	147.3	36.4	314.6	0.0	498.2	69.4	126.2	17.6	0.0	0.0	72.0	10.0	72.0	10.0	12.8	1.8	0.0	0.0	8.2	1.1
1803	-26.913595	150.988028	10:39:22	335	1.842	-47.4	83.6	0.0	0.0	0.0	0.0	0.0	0.0	8.0	9.6	58.9	70.4	0.0	0.0	58.9	70.4	7.4	8.8	0.0	0.0	9.3	11.1
1804	-26.777345	150.728169	10:50:02	309	1.841	-47.4	61.0	0.0	0.0	0.0	0.0	0.0	0.0	0.0	0.0	58.9	96.6	0.0	0.0	58.9	96.6	0.0	0.0	0.0	0.0	2.1	3.4
1805	-26.674329	150.462714	11:00:57	289	1.845	-47.5	28.1	0.4	0.0	0.0	0.0	0.4	1.0	0.0	0.0	19.6	69.9	6.5	23.3	26.2	93.1	0.0	0.0	0.0	0.0	1.5	5.5
1806	-26.631331	150.296620	11:07:21	279	1.839	-47.5	2.7	0.8	0.0	0.0	0.0	0.8	28.0	0.0	0.0	0.0	0.0	0.0	0.0	0.0	0.0	0.0	0.0	0.0	0.0	2.0	71.8
1808	-26.849174	150.720908	11:39:13	155	1.846	-47.5	62.0	0.4	0.0	0.0	0.0	0.4	1.0	0.0	0.0	58.9	95.0	0.0	0.0	58.9	95.0	0.0	0.0	0.0	0.0	2.7	4.4
1809	-27.013423	150.968222	11:49:35	149	1.850	-47.4	31.4	0.4	0.0	0.0	0.0	0.4	1.0	0.0	0.0	13.1	41.7	0.0	0.0	13.1	41.7	7.4	23.5	0.0	0.0	10.6	33.6
1810	-27.159376	151.171367	11:58:21	137	1.842	-47.4	67.4	0.0	0.0	0.0	0.0	0.0	0.0	5.6	8.3	32.7	48.5	0.0	0.0	32.7	48.5	7.0	10.5	0.0	0.0	7.0	10.5
1811	-27.252709	151.290522	12:03:32	149	1.843	-47.5	220.6	0.0	0.0	0.0	0.0	0.0	0.0	120.5	54.7	32.7	14.8	0.0	0.0	32.7	14.8	55.9	25.3	0.0	0.0	11.4	5.2
1814	-27.477124	151.346706	13:57:52	280	1.846	-47.5	6.5	0.8	0.0	0.0	0.0	0.8	12.0	0.0	0.0	0.0	0.0	0.0	0.0	0.0	0.0	0.0	0.0	0.0	0.0	5.8	88.2
1815	-27.362967	151.053722	14:10:10	287	1.843	-47.5	430.8	122.1	15.8	251.6	0.0	389.6	90.0	0.0	0.0	39.3	9.1	0.0	0.0	39.3	9.1	0.0	0.0	0.0	0.0	2.0	0.5
1816	-27.270302	150.861734	14:18:00	302	1.847	-47.3	971.3	89.1	54.9	251.6	148.5	544.1	56.0	0.0	0.0	13.1	1.3	0.0	0.0	13.1	1.3	408.2	42.0	0.0	0.0	5.9	0.6
1817	-27.277108	150.523147	14:30:02	293	1.844	-47.4	1291.6	136.4	581.9	459.2	77.9	1255.5	97.0	0.0	0.0	32.7	2.5	0.0	0.0	32.7	2.5	2.5	0.2	0.0	0.0	0.4	0.1
1818	-27.300287	150.255494	14:38:58	288	1.851	-47.4	320.3	141.5	0.0	0.0	99.8	241.3	75.0	0.0	0.0	78.5	24.5	0.0	0.0	78.5	24.5	0.0	0.0	0.0	0.0	0.4	0.1
1819	-26.818757	150.085653	14:56:06	134	1.838	-47.8	326.1	0.0	0.0	0.0	0.0	0.0	0.0	200.9	61.6	124.4	38.1	0.0	0.0	124.4	38.1	0.0	0.0	0.0	0.0	0.8	0.2
1820	-27.318757	150.296830	15:03:46	131	1.850	-47.6	336.0	123.2	0.0	125.8	0.0	249.1	74.0	8.0	2.4	78.5	23.4	0.0	0.0	78.5	23.4	0.0	0.0	0.0	0.0	0.3	0.1
1821	-27.329988	150.549739	15:13:02	152	1.854	-47.7	352.2	58.5	25.5	251.6	0.0	335.7	95.0	0.0	0.0	13.1	3.7	0.0	0.0	13.1	3.7	2.5	0.7	0.0	0.0	0.9	0.3
1822	-27.355856	150.895895	15:25:37	145	1.848	-47.6	918.9	143.8	73.2	251.6	223.5	692.1	75.0	192.9	21.0	13.1	1.4	0.0	0.0	13.1	1.4	5.6	0.6	0.0	0.0	15.3	1.7
1823	-27.413887	151.002427	15:29:53	150	1.844	-47.6	367.1	159.7	47.9	125.8	0.0	333.4	90.0	0.0	0.0	8.9	8.9	32.7	8.9	32.7	8.9	0.0	0.0	0.0	0.0	1.0	0.3
1825	-27.488623	151.315303	15:41:09	134	1.847	-47.5	6.9	1.2	0.0	0.0	0.0	1.2	17.0	0.0	0.0	0.0	0.0	0.0	0.0	0.0	0.0	0.0	0.0	0.0	0.0	5.8	83.2
1903	-26.601911	150.209547	11:28:42	143	1.847	-47.4	172.2	24.8	0.0	0.0	0.0	24.8	14.0	8.0	4.7	0.0	0.0	137.4	79.8	137.4	79.8	0.0	0.0	0.0	0.0	1.9	1.1
1904	-26.666918	150.087434	11:33:30	153	1.843	-47.4	157.7	18.2	0.0	0.0	0.0	18.2	12.0	0.0	0.0	0.0	0.0	137.4	87.2	137.4	87.2	0.0	0.0	0.0	0.0	2.0	1.3
1905	-26.812782	150.387755	11:59:39	298	1.843	-47.4	336.8	61.2	8.6	125.8	0.0	195.6	58.0	48.1	14.3	0.0	0.0	91.6	27.2	91.6	27.2	0.0	0.0	0.0	0.0	1.5	0.4
1906	-26.849103	150.531985	12:08:28	145	1.851	-47.8	42.1	1.2	0.0	0.0	0.0	1.2	3.0	0.0	0.0	0.0	0.0	39.3	93.2	39.3	93.2	0.0	0.0	0.0	0.0	1.7	4.1
1907	-26.929175	150.172493	12:22:54	150	1.848	-47.6	119.9	14.0	0.0	0.0	0.0	14.0	12.0	0.0	0.0	0.0	0.0	104.7	87.4	104.7	87.4	0.0	0.0	0.0	0.0	1.2	1.0
1908	-27.058387	150.472602	12:46:44	286	1.850	-47.3	1740.0	305.0	214.9	761.2	311.3	1592.4	92.0	48.2	2.8	0.0	0.0	72.0	4.1	72.0	5.3	0.0	0.0	0.0	0.0	7.7	0.4
1909	-26.904910	150.697134	12:59:31	169	1.843	-47.4	96.4	5.0	0.0	0.0	0.0	5.0	5.0	0.0	0.0	0.0	0.0	72.0	74.7	72.0	74.7	0.0	0.0	0.0	0.0	19.4	20.1
1910	-27.082716	150.444703	13:10:43	110	1.846	-47.5	2057.4	320.9	210.0	905.9	380.0	1816.9	88.0	167.1	8.1	0.0	0.0	65.4	3.2	65.4	3.2	0.0	0.0	0.0	0.0	8.0	0.4
1911	-27.172024	150.324018	13:16:03	142	1.845	-47.4	221.4	61.2	0.0	0.0	0.0	61.2	28.0	8.0	3.6	0.0	0.0	150.5	68.0	150.5	68.0	0.0	0.0	0.0	0.0	1.6	0.7
1912	-27.389992	151.211960	14:54:55	321	1.847	-47.4	1325.4	286.4	32.6	251.6	75.0	645.7	49.0	192.9	14.6	45.8	3.5	13.1	1.0	58.9	4.4	408.2	30.8	0.0	0.0	19.8	1.5
1914	-27.306893	151.290365	15:01:45	155	1.849	-47.5	313.3	65.1	18.3	62.9	21.4	167.8	54.0	0.0	0.0	0.0	0.0	0.0	0.0	0.0	0.0	130.5	41.7	0.0	0.0	14.9	4.8
1915	-27.573146	151.046142	15:15:34	140	1.845	-47.6	198.3	57.0	13.3	0.0	0.0	70.2	35.0	27.3	13.8	0.0	0.0	58.9	29.7	58.9	29.7	5.6	2.9	0.0	0.0	1.6	0.8
1917	-27.481054	151.127999	15:22:42	300	1.848	-47.4	897.7	225.2	101.8	220.2	276.8	823.9	92.0	27.3	3.0	0.0	0.0	26.2	2.9	26.2	2.9	5.6	0.6	0.0	0.0	16.1	1.8
1918	-27.413731	151.121276	15:27:42	280	1.848	-47.6	713.0	19.4	0.0	0.0	0.0	19.4	3.0	574.6	80.6	45.8	6.4	0.0	0.0	45.8	6.4	26.1	3.7	0.0	0.0	47.1	6.6
2101	-27.410985	151.117254	9:49:40	155	1.844	-47.6	690.9	22.9	0.0	0.0	0.0	22.9	3.0	570.6	82.6	39.3	5.7	0.0	0.0	39.3	5.7	18.4	2.7	0.0	0.0	39.7	5.7
2102	-27.001783	150.264342	12:04:27	282	1.863	-48.0	1971.2	251.9	586.3	714.0	339.0	1891.3	96.0	0.0	0.0	26.2	1.3	0.0	0.0	78.5	4.0	0.0	0.0	0.0	0.0	1.4	0.1
2103	-26.883722	150.808471	14:06:26	200	1.850	-47.5	608.7	60.5	18.3	62.9	75.0	216.7	36.0	5.6	0.9	58.9	16.1	26.2	7.2	85.1	23.3	0.0	0.0	0.0	0.0	40.3	6.6
2105	-26.602870	150.306461	14:06:26	157	1.850	-47.5	365.3	25.6	0.0	0.0	0.0	25.6	7.0	0.0	0.0	58.9	16.1	26.2	7.2	85.1	23.3	0.0	0.0	237.6	65.0	17.1	4.7
2107	-26.633661	150.225549	14:09:23	137	1.852	-47.6	487.0	109.3	8.6	188.7	0.0	306.6	63.0	0.0	0.0	52.4	10.8	52.4	10.8	104.7	21.5	0.0	0.0	0.0	0.0	75.7	15.5
2108	-26.593793	150.350332	14:44:23	280	1.848	-47.6	363.1	9.7	0.0	0.0	0.0	9.7	3.0	0.0	0.0	78.5	21.6	19.6	5.4	98.2	27.0	0.0	0.0	237.6	65.4	17.6	4.9
2110	-26.868780	150.297704	15:00:41	290	1.859	-47.6	2209.1	244.9	787.5	811.5	210.7	2054.6	93.0	88.2	4.0	0.0	0.0	39.3	1.8	39.3	1.8	0.0	0.0	0.0	0.0	0.8	0.0
2112	-26.930582	150.496868	15:14:29	299	1.844	-47.5	514.1	120.5	22.4	15.7	0.0	158.6	30.8	0.0	0.0	19.6	3.8	26.2	5.1	45.8	8.9	307.6	59.8	0.0	0.0	2.1	0.4

Legend

- Coal Mines > 50% BTF BU Inventory
- Piggeries > 50% BTF BU Inventory
- Coal Seam Gas > 50% BTF BU inventory, 250 m to 350 m
- Coal Seam Gas > 50% BTF BU inventory, 100 m to 200 m
- Grazing Cattle > 50% BTF BU inventory, 250 m to 350 m
- Grazing Cattle > 50% BTF BU inventory, 100 m to 200 m
- Feedlots > 50% BTF BU inventory, 250 m to 350 m
- Feedlots > 50% BTF BU inventory, 100 m to 200 m
- Mixed Sources
- Outliers
- Points of Interest with low δ^{13}C-CH$_4$ readings

Table A4. Calculated $\delta^{13}C_{CH4(s)}$ values using multi-Keeling-model regression with shared $CH_{4(b)}$ and $\delta^{13}C_{CH4(b)}$ and using multi-Miller-Tans-model regression with shared $CH_{4(b)}$ and $\delta^{13}C_{CH4(b)}$.

Category Data Set	Parameter	Multi-Keeling-Model Shared $CH_{4(b)}$ and $\delta^{13}C_{CH4(b)}$ (Eq. 1)				Multi-Miller-Tans-Model with Shared $CH_{4(b)}$ and $\delta^{13}C_{CH4(b)}$ (Eq. 3)			
		Estimate	Standard Error	Confidence Interval (95 %) Lower Bound	Confidence Interval (95 %) Upper Bound	Estimate	Standard Error	Confidence Interval (95 %) Lower Bound	Confidence Interval (95 %) Upper Bound
Background Air	$CH_{4(b)}$ (ppm)	1.825	0.018	1.788	1.863	1.825	0.018	1.787	1.863
Background Air	$\delta^{13}C_{CH4(b)}$ (‰)	-47.3	0.1	-47.6	-47.0	-47.3	0.1	-47.6	-47.0
Coal Seam Gas >50 % BTF BU inventory, 100–200 mAGL	$\delta^{13}C_{CH4(s)}$ (‰)	-65.3	6.4	-78.5	-52.2	-65.4	6.4	-78.5	-52.2
Coal Seam Gas >50 % BTF BU inventory, 250–350 mAGL	$\delta^{13}C_{CH4(s)}$ (‰)	-55.5	6.5	-68.9	-42.1	-55.6	6.5	-69.0	-42.3
Grazing Cattle >50 % BTF BU inventory, 100–200 mAGL	$\delta^{13}C_{CH4(s)}$ (‰)	-52.5	9.1	-71.3	-33.7	-52.6	9.1	-71.4	-33.8
Grazing Cattle >50 % BTF BU inventory, 250–350 mAGL	$\delta^{13}C_{CH4(s)}$ (‰)	-60.5	7.4	-75.7	-45.4	-60.6	7.4	-75.8	-45.5
Feedlots >50 % BTF BU inventory, 100–350 mAGL	$\delta^{13}C_{CH4(s)}$ (‰)	-69.5	10.7	-91.6	-47.4	-69.5	10.8	-91.6	-47.4

Atmospheric Chemistry and Physics Discussions — Open Access, EGU

Table A5. Single point confidence interval statistics for multi-Keeling-model regression with shared $CH_{4(b)}$ and $\delta^{13}C_{CH4(b)}$ and multi-Miller-Tans-model regression with shared $CH_{4(b)}$ and $\delta^{13}C_{CH4(b)}$.

Category Data Set	Multi-Keeling-Model Regression with Shared $CH_{4(b)}$ and $\delta^{13}C_{CH4(b)}$						Multi-Miller-Tans-Model Regression with Shared $CH_{4(b)}$ and $\delta^{13}C_{CH4(b)}$					
	Observed	Predicted	Standard Error	Single Prediction Confidence Interval (95 %) Lower Bound	Single Prediction Confidence Interval (95 %) Upper Bound	Single Prediction Confidence Interval (95 %) 1/2 Interval	Observed	Predicted	Standard Error	Single Prediction Confidence Interval (95 %) Lower Bound	Single Prediction Confidence Interval (95 %) Upper Bound	Single Prediction Confidence Interval (95 %) 1/2 Interval
	$\delta^{13}C_{CH4(b)}$	$\delta^{13}C_{CH4}$					$\delta^{13}C_{CH4(b)}\cdot CH_4$	$\delta^{13}C_{CH4(b)}\cdot CH_4$				
Coal Seam Gas >50 % BTF BU inventory, 100–200 mAGL	-47.59	-47.57	0.06	-47.70	-47.44	0.13	-87.27	-87.16	0.13	-87.42	-86.90	0.26
	-47.66	-47.61	0.07	-47.74	-47.47	0.14	-87.70	-87.55	0.12	-87.79	-87.32	0.24
	-47.56	-47.55	0.06	-47.68	-47.42	0.13	-87.51	-87.39	0.12	-87.64	-87.15	0.24
	-47.61	-47.52	0.06	-47.65	-47.38	0.13	-87.40	-87.60	0.12	-87.84	-87.37	0.24
	-47.53	-47.55	0.06	-47.68	-47.42	0.13	-87.45	-87.45	0.12	-87.69	-87.21	0.24
	-47.45	-47.54	0.06	-47.67	-47.41	0.13	-87.78	-87.80	0.12	-88.04	-87.56	0.24
	-47.51	-47.56	0.06	-47.69	-47.43	0.13	-87.42	-87.39	0.12	-87.64	-87.15	0.24
	-47.59	-47.59	0.07	-47.73	-47.46	0.13	-87.52	-87.74	0.12	-87.98	-87.50	0.24
					Average	**0.13**					**Average**	**0.24**
Coal Seam Gas >50 % BTF BU inventory, 250–350 mAGL	-47.45	-47.39	0.07	-47.53	-47.25	0.14	-87.53	-87.64	0.12	-87.87	-87.40	0.24
	-47.50	-47.42	0.06	-47.55	-47.30	0.13	-88.41	-88.24	0.14	-88.52	-87.96	0.28
	-47.47	-47.41	0.06	-47.54	-47.28	0.13	-88.04	-88.00	0.12	-88.25	-87.76	0.24
	-47.32	-47.43	0.06	-47.56	-47.30	0.13	-88.35	-88.26	0.12	-88.51	-88.01	0.25
	-47.41	-47.42	0.06	-47.55	-47.29	0.13	-87.89	-87.89	0.12	-88.13	-87.65	0.24
	-47.44	-47.44	0.06	-47.57	-47.31	0.13	-87.81	-87.84	0.12	-88.08	-87.60	0.24
	-47.32	-47.44	0.06	-47.57	-47.31	0.13	-87.61	-87.77	0.12	-88.01	-87.53	0.24
	-47.37	-47.43	0.06	-47.56	-47.30	0.13	-87.85	-87.95	0.12	-88.19	-87.71	0.24
	-47.57	-47.48	0.07	-47.63	-47.32	0.15	-88.14	-88.16	0.12	-88.40	-87.91	0.25
					Average	**0.13**					**Average**	**0.25**
Grazing Cattle >50 % BTF BU inventory, 100–200 mAGL	-47.48	-47.39	0.07	-47.53	-47.26	0.14	-87.44	-87.41	0.12	-87.66	-87.16	0.25
	-47.35	-47.39	0.07	-47.53	-47.26	0.14	-87.41	-87.43	0.12	-87.68	-87.18	0.25
	-47.39	-47.39	0.07	-47.53	-47.26	0.14	-87.30	-87.32	0.12	-87.56	-87.07	0.25
	-47.44	-47.38	0.07	-47.52	-47.25	0.13	-87.59	-87.58	0.13	-87.84	-87.32	0.26
	-47.38	-47.39	0.06	-47.52	-47.25	0.13	-87.46	-87.53	0.12	-87.78	-87.28	0.25
					Average	**0.14**					**Average**	**0.25**
Grazing Cattle >50 % BTF BU inventory, 250–350 mAGL	-47.46	-47.45	0.07	-47.59	-47.32	0.14	-87.54	-87.54	0.12	-87.79	-87.29	0.25
	-47.44	-47.45	0.07	-47.59	-47.32	0.14	-87.67	-87.58	0.12	-87.84	-87.33	0.25
	-47.43	-47.44	0.07	-47.57	-47.31	0.13	-87.32	-87.31	0.12	-87.56	-87.07	0.25
	-47.48	-47.47	0.07	-47.61	-47.33	0.14	-87.38	-87.41	0.12	-87.66	-87.16	0.25
					Average	**0.14**					**Average**	**0.25**
Feedlots >50 % BTF BU inventory, 100–350 mAGL	-47.60	-47.62	0.07	-47.77	-47.47	0.15	-88.04	-88.08	0.13	-88.35	-87.80	0.27
	-47.48	-47.54	0.06	-47.67	-47.40	0.13	-87.48	-87.59	0.12	-87.84	-87.34	0.25
	-47.49	-47.55	0.06	-47.68	-47.41	0.13	-87.54	-87.65	0.12	-87.89	-87.40	0.24
	-47.52	-47.48	0.07	-47.63	-47.33	0.15	-87.34	-87.28	0.13	-87.56	-87.00	0.28
	-47.64	-47.60	0.07	-47.74	-47.46	0.14	-88.04	-87.96	0.13	-88.21	-87.70	0.26
	-47.61	-47.55	0.06	-47.68	-47.42	0.13	-87.79	-87.67	0.12	-87.92	-87.43	0.24
					Average	**0.14**					**Average**	**0.26**
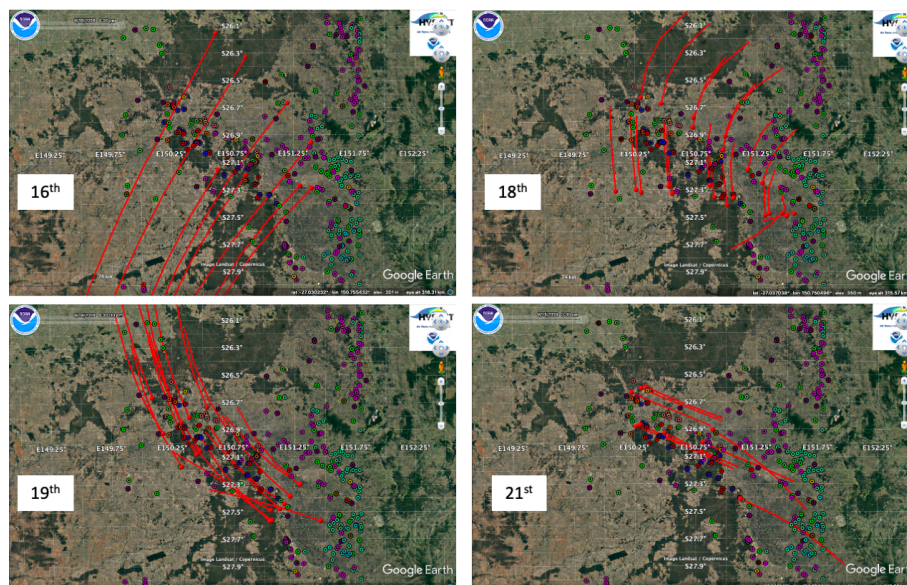
Point Sources

🔴 CSG processing plants	🟢 Cattle feedlots
🟠 CSG compressor stations	🟢 Cattle dairy
🔵 CSG raw water ponds	🟣 Piggeries
⚪ Coal mines	🔵 Poultry farms
🩷 Power stations	🟤 Landfills
🌸 Ground seeps	🟤 Wastewater treatment plants
🟡 River gas seeps	🟢 Domestic wood fires

845 **Figure A1.** Three-hour HYSPLIT back-trajectory path lines (red) for each day of IFAA sampling. The back-trajectory starts at the mid-point of the air sample collection interval (circled end of the red line) (image ©Google Earth).
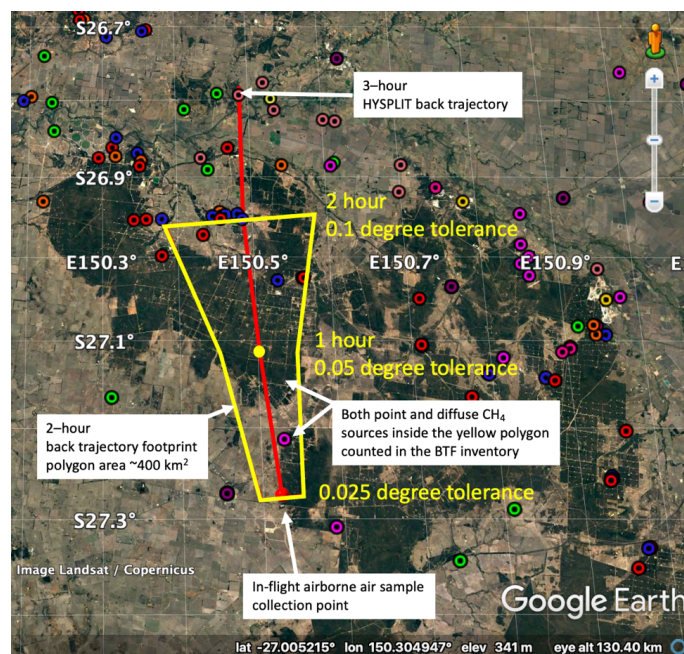
850 **Figure A2.** A representative BTF inventory polygon for IFAA sample 1817. Refer to Fig. A1 for the point source colour key (image ©Google Earth).
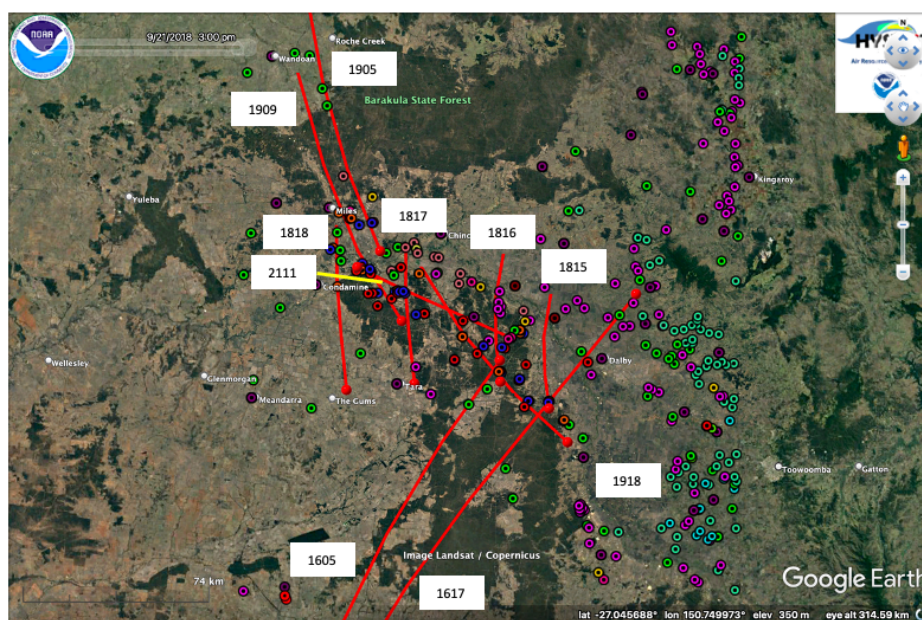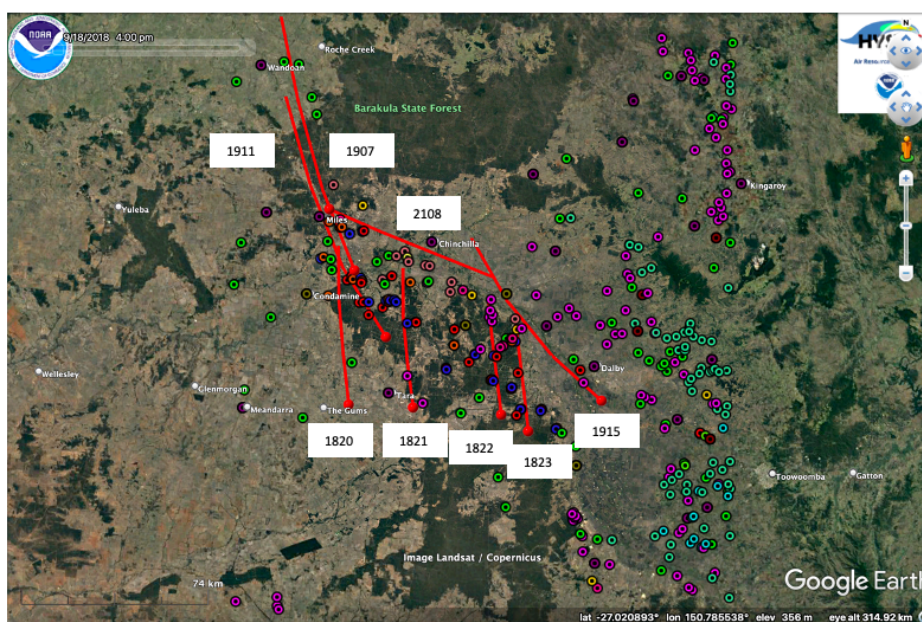
Figure A3. Three-hour HYSPLIT back-trajectory path lines (red) for the points used in the coal seam gas Keeling-model regression analysis. Refer to Fig. A1 for the point source colour key (image ©Google Earth).
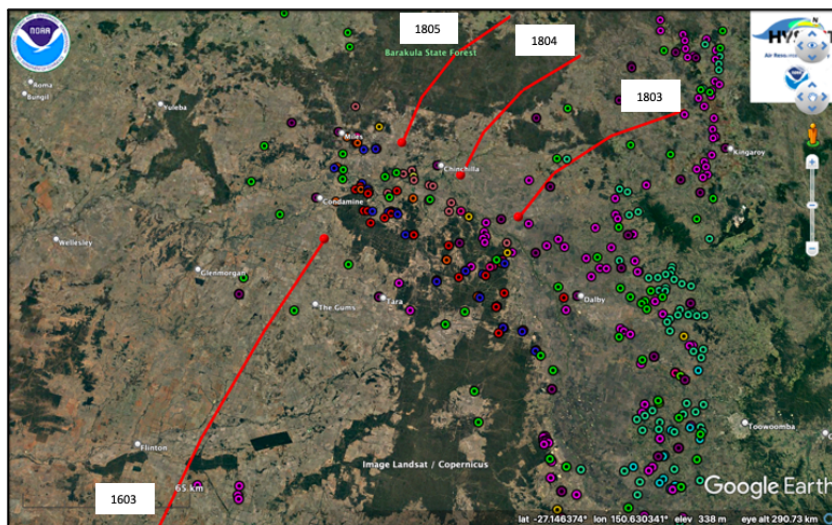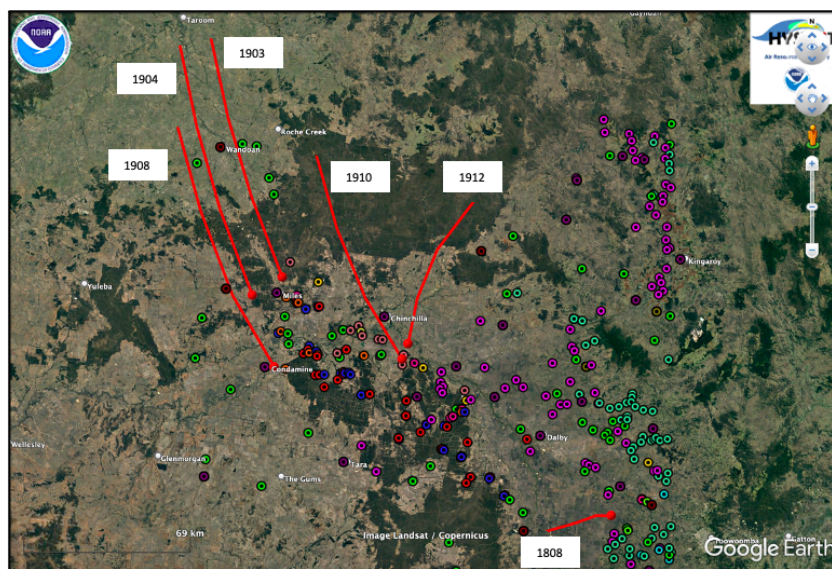
Figure A4. Three-hour HYSPLIT back-trajectory path lines (red) for the points used in the grazing cattle Keeling-model regression analysis. Refer to Fig. A1 for the point source colour key (image ©Google Earth).
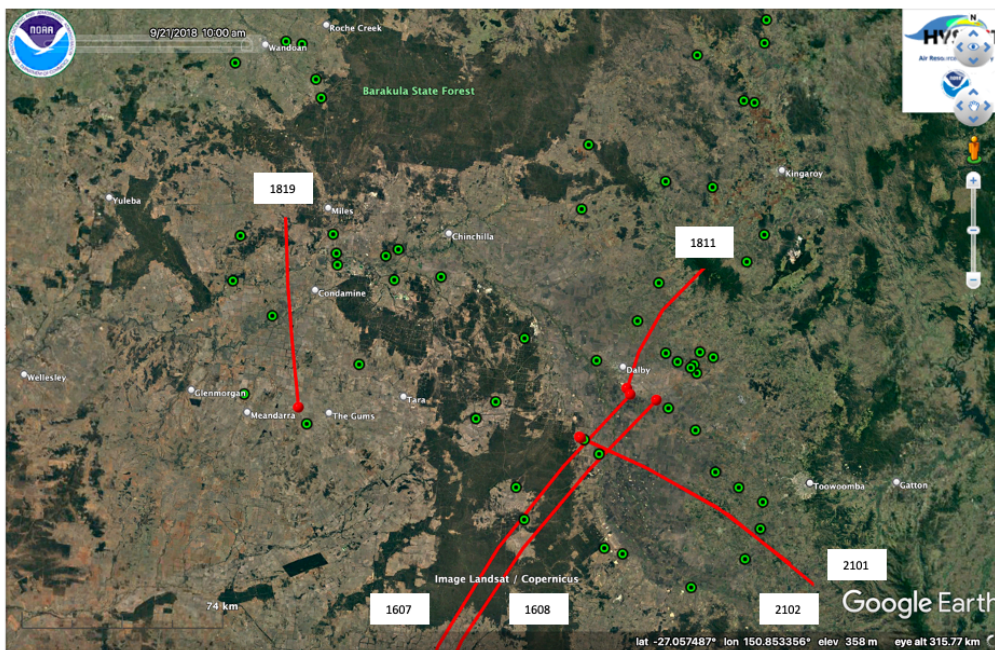
Figure A5. Three-hour HYSPLIT back-trajectory path lines (red) for the points used in the feedlot Keeling-model regression analysis.
865   Each green dot indicates the position of a feedlot (image ©Google Earth).

Appendix B

A commonly used method to determine $\delta^{13}C_{CH4(s)}$ is to fit the Keeling model (Eq. 1) or Miller-Tans model (Eq. 2) to a set of air samples collected with a single plume. For the IFAA samples collected as part of this study the combination of the low level of CH_4 enhancement (< 0.040 ppm) and the small number of samples in each category (< 10 IFAA samples) results in poorly constrained regressions with large uncertainties (Table B1).

Table B1. Calculated $\delta^{13}C_{CH4(s)}$ values for Keeling model (Eq. 1) and Miller-Tans model (Eq. 2) fitted to the individual source category data sets.

Category Data Set	Parameter	Individual Keeling-Model Regression (Eq. 1)				Individual Miller-Tans-Model Regression (Eq..2)			
		Estimate	Standard Error	Confidence Interval (95 %) Lower Bound	Confidence Interval (95 %) Upper Bound	Estimate	Standard Error	Confidence Interval (95 %) Lower Bound	Confidence Interval (95 %) Upper Bound
Coal Seam Gas >50 % BTF BU inventory, 100–200 mAGL	$\delta^{13}C_{CH4(s)}$ (‰)	-66.8	14.9	-105.0	-28.6	-66.9	14.8	-105.0	-28.7
Coal Seam Gas >50 % BTF BU inventory, 250–350 mAGL	$\delta^{13}C_{CH4(s)}$ (‰)	-54.6	10.1	-78.4	-30.7	-54.7	10.1	-78.5	-30.9
Grazing Cattle >50 % BTF BU inventory, 100–200 mAGL	$\delta^{13}C_{CH4(s)}$ (‰)	-60.0	18.4	-139.1	19.2	-60.0	18.4	-139.2	19.3
Grazing Cattle >50 % BTF BU inventory, 250–350 mAGL	$\delta^{13}C_{CH4(s)}$ (‰)	-65.3	11.5	-211.5	80.8	-65.3	11.5	-211.4	80.7
Feedlots >50 % BTF BU inventory, 100–350 mAGL	$\delta^{13}C_{CH4(s)}$ (‰)	-68.9	14.1	-113.8	-24.0	-69.0	14.1	-113.8	-24.1

The single category Keeling model (Eq. 1) results are presented in Fig. B1 (a) to highlight the issue of fitting the Keeling model to small data sets with low CH_4 enhancement above background $CH_{4(b)}$. The Keeling regression lines in Fig. B1 (a) do not converge to a common point for $CH_{4(b)}$ and $\delta^{13}C_{CH4(b)}$ as would be expected given the stability of $CH_{4(b)}$ established during the continuous measurement airborne campaign (Neininger et al. 2021). Many of the regression lines converge far to the right of the $CH_{4(b)}$ and $\delta^{13}C_{CH4(b)}$ values determined from the simultaneous multiple regression. In addition, the uncertainty bars for the source signatures derived from the unconstrained fits are so large that no meaningful source attribution is possible (Table B1). The resulting $\delta^{13}C_{CH4(s)}$ signatures of the individual regressions for each category are: *CSG >50% BTF BU inventory, 100–200 mAGL*, −66.8 ‰ (CI 95 % ± 38.2 ‰); *CSG >50% BTF BU inventory, 250–350 mAGL*, −54.6 ‰ (CI 95 % ± 23.9 ‰); *Grazing Cattle >50% BTF BU inventory, 100–200 mAGL*, −60.0 ‰ (CI 95 % ± 79.2 ‰); *Grazing Cattle >50% BTF BU inventory, 250–350 mAGL*, −65.3 ‰ (CI 95 % ± 146.1 ‰); and *Feedlots >50 % BTF BU inventory, 100–350 mAGL*, −68.9 ‰ (CI 95 % ± 44.9 ‰).

When $CH_{4(b)}$ and $\delta^{13}C_{CH4(b)}$ are unknown, it is common to use the Miller-Tans model (Eq. 2) to determine $\delta^{13}C_{CH4(s)}$. The results of fitting this model separately to the five category data sets are presented in Fig. B1 (b). Like the Keeling model the regression lines of best fit do not converge to a common point for $CH_{4(b)}$ and $\delta^{13}C_{CH4(b)}$. The 95 % confidence intervals are also large (Table B1). The resulting $\delta^{13}C_{CH4(s)}$ signatures of the individual regressions for each category are: *CSG >50 % BTF BU inventory, 100–200 mAGL*, −66.9 ‰ (CI 95 % ± 38.1 ‰); *CSG >50 % BTF BU inventory, 250–350 mAGL*, −54.7 ‰ (CI 95 % ± 23.8 ‰); *Grazing Cattle >50 % BTF BU inventory, 100–200 mAGL*, −60.0 ‰ (CI 95 % ± 79.2 ‰); *Grazing Cattle >50% BTF BU inventory, 250–350 mAGL*, −65.3 ‰ (CI 95 % ± 146.1 ‰); and *Feedlots >50 % BTF BU inventory, 100–350 mAGL*, −69.0 ‰ (CI 95 % ± 44.9 ‰).

900 These poorly constrained results highlight why multi-Keeling-model regression was used for this study to better constrain the interpretation of the IFAA samples. As previously stated in the main text, the multi-Keeling-model regression determined values for $CH_{4(b)}$ and $\delta^{13}C_{CH4(b)}$ represent the background air centroid for all days of measurements, which is useful knowledge, as it highlights that none of the IFAA samples represented background air. Comparing the derived $\delta^{13}C_{CH4(b)}$ values in Tables A3 and B1 there is little variation in source signatures for each category regardless of which two-endmember mixing model

905 was used or regression method applied.
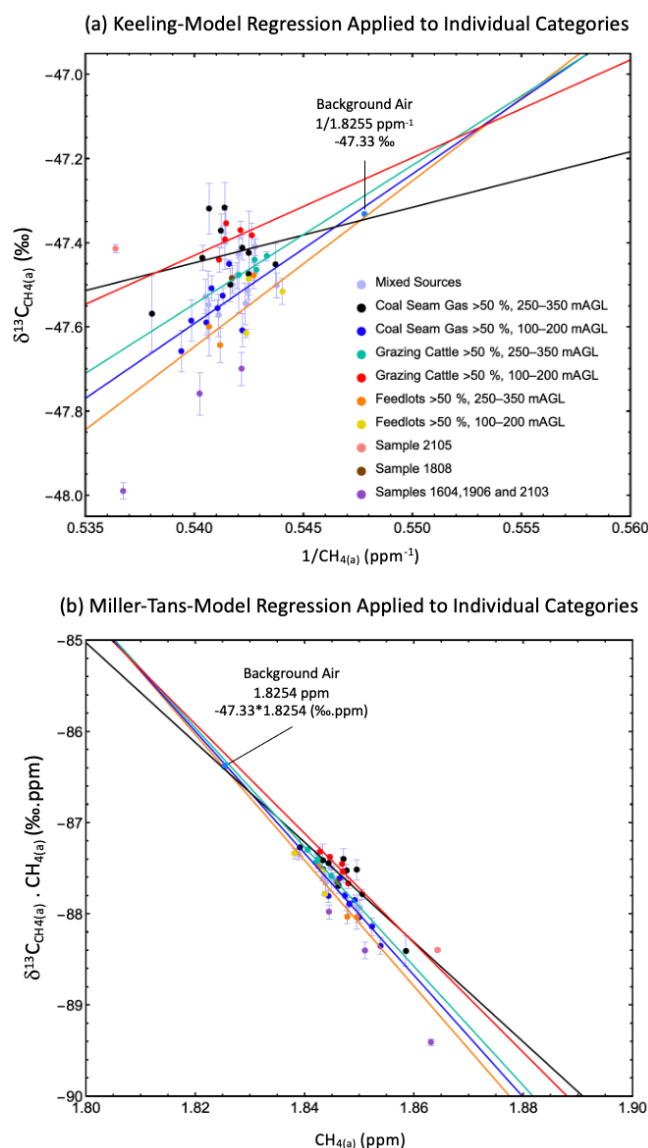
Figure B1. Least squares regression for two-endmember mixing models fitted to individual source category data sets using (a) the Keeling model (Eq. 1) and (b) the Miller-Tans model (Eq. 2). For reference the background air values for $CH_{4(b)}$ and $\delta^{13}C_{CH4(b)}$ determined from the

910 multi-Keeling and multi-Miller-Tans model regressions are displayed in plots (a) and (b), respectively. The regression statistics for each category are listed in Table B1. Both graphs highlight that when the models are fitted to the individual source category data sets the lines of best fit do not converge to a common value for background air.

References

915

Albers, J.C., Kiers, H.A.L., and van Ravenzwaaij, D.: Credible confidence: a pragmatic view on the frequentist vs Bayesian debate. Collabra: Psychology, 4(1): 31. DOI: https://doi.org/10.1525/collabra.149, 2018.

Australian Competition and Consumer Commission: Gas inquiry 2017-2025 Interim report., [online] Avaialbe from https://www.accc.gov.au/publications/serial-publications/gas-inquiry-2017-2025 (Accessed 17 January 2022), 2020.

920 Australian Government: National Inventory Report 2018 Volume 1., [online] Available from: https://www.industry.gov.au/data-and-publications/national-greenhouse-gas-inventory-report-2018 (Accessed 17 Jan 2020), 2020a.

Australian Government: Quarterly Update of Australia's National Greenhouse Gas Inventory: September 2020.,[online] Available from https://www.industry.gov.au/data-and-publications/national-greenhouse-gas-inventory-quarterly-updates

925 (Accessed 17 January 2022), 2020b.

Australian Government, 2021 National Gas Infrastructure Plan. Department of Industry, Science, Energy and Resources. Available from: https://www.energy.gov.au/sites/default/files/2021%20National%20Gas%20Infrastructure%20Plan.pdf (Accessed 17 January 2002), 2021

Barkley, Z. R., Lauvaux, T., Davis, K. J., Deng, A., Miles, N. L., Richardson, S. J., Cao, Y., Sweeney, C., Karion, A., Smith,

930 M., Kort, E. A., Schwietzke, S., Murphy, T., Cervone, G., Martins, D. and Maasakkers, J. D.: Quantifying methane emissions from natural gas production in north-eastern Pennsylvania, Atmos. Chem. Phys., 17(22), 13941–13966, doi:10.5194/acp-17-13941-2017, 2017.

Basu, S., Lan, X., Dlugokencky, E., Michel, S., Schwietzke, S., Miller, J. B., Bruhwiler, L., Oh, Y., Tans, P. P., Apadula, F., Gatti, L. V., Jordan, A., Necki, J., Sasakawa, M., Morimoto, S., Di Iorio, T., Lee, H., Arduini, J., and Manca, G.:

935 Estimating Emissions of Methane Consistent with Atmospheric Measurements of Methane and δ^{13}C of Methane, Atmos. Chem. Phys. Discuss. [preprint], https://doi.org/10.5194/acp-2022-317, in review, 2022.

Baublys, K. A., Hamilton, S. K., Golding, S. D., Vink, S. and Esterle, J.: Microbial controls on the origin and evolution of coal seam gases and production waters of the Walloon Subgroup; Surat Basin, Australia, Int. J. Coal Geol., 147–148, 85–104, doi:10.1016/j.coal.2015.06.007, 2015.

940 Beck, V., Chen, H., Gerbig, C., Bergamaschi, P., Bruhwiler, L., Houweling, S., Röckmann, T., Kolle, O., Steinbach, J., Koch, T., Sapart, C. J., Veen, C. van der, Frankenberg, C., Andreae, M. O., Artaxo, P., Longo, K. M. and Wofsy, S. C.: Methane airborne measurements and comparison to global models during BARCA, J. Geophys. Res. Atmos., 117(D15), 15310, doi:10.1029/2011JD017345, 2012.

Day, C., Tibbett, S., Sestak, A., Knight, S., Marvig, C., Mcgarry, P., Weir, S., White, S., Armand, S., Van Holst, S., Fry, J.,

945 Dell'amico, R., Halliburton, M. and Azzi, B.: Methane and Volatile Organic Compound Emissions in New South Wales., 2016.

Desjardins, R. L., Worth, D. E., Pattey, E., VanderZaag, A., Srinivasan, R., Mauder, M., Worthy, D., Sweeney, C. and Metzger, S.: The challenge of reconciling bottom-up agricultural methane emissions inventories with top-down measurements, Agric. For. Meteorol., 248, 48–59, doi:10.1016/J.AGRFORMET.2017.09.003, 2018.

950 Dlugokencky, E. J., Myers, R. C., Lang, P. M., Masarie, K. A., Crotwell, A. M., Thoning, K. W., Hall, B. D., Elkins, J. W. and Steele, L. P.: Conversion of NOAA atmospheric dry air CH_4 mole fractions to a gravimetrically prepared standard scale, J. Geophys. Res. D Atmos., 110(18), 1–8, doi:10.1029/2005JD006035, 2005.

Draper, J. J. and Boreham, C. J.: Geological Controls On Exploitable Coal Seam Gas Distribution In Queensland, APPEA J., 46(1), 366, doi:10.1071/aj05019, 2006.

955 Draxler, R. R., Spring, S., Maryland, U. S. A. and Hess, G. D.: An Overview of the HYSPLIT_4 Modelling System for Trajectories, Dispersion, and Deposition, Aust. Meteorol. Mag., 47, 295–308, 1998.

EFDB: Change., Emission Factor Database EFDB. IPCC - Intergovernmental Panel on Climate, [online] Available from: https://www.ipcc-nggip.iges.or.jp/EFDB/main.php (Accessed 23 August 2021), 2006.

Fisher, R., Lowry, D., Wilkin, O., Sriskantharajah, S. and Nisbet, E. G.: High-precision, automated stable isotope analysis of

960 atmospheric methane and carbon dioxide using continuous-flow isotope-ratio mass spectrometry, Rapid Commun. Mass Spectrom., 20(2), 200–208, doi:10.1002/rcm.2300, 2006.

Fisher, R. E., France, J. L., Lowry, D., Lanoisellé, M., Brownlow, R., Pyle, J. A., Cain, M., Warwick, N., Skiba, U. M., Drewer, J., Dinsmore, K. J., Leeson, S. R., Bauguitte, S. J. -B., Wellpott, A., O'Shea, S. J., Allen, G., Gallagher, M. W., Pitt, J., Percival, C. J., Bower, K., George, C., Hayman, G. D., Aalto, T., Lohila, A., Aurela, M., Laurila, T., Crill, P. M.,

965 McCalley, C. K. and Nisbet, E. G.: Measurement of the ^{13}C isotopic signature of methane emissions from northern European wetlands, Global Biogeochem. Cycles, 31(3), 605–623, doi:10.1002/2016GB005504@10.1002/(ISSN)2169-9291.ARCTICJOINT, 2017.

France, J. L., Cain, M., Fisher, R. E., Lowry, D., Allen, G., O'Shea, S. J., Illingworth, S., Pyle, J., Warwick, N., Jones, B. T., Gallagher, M. W., Bower, K., Le Breton, M., Percival, C., Muller, J., Welpott, A., Bauguitte, S., George, C., Hayman, G.

970 D., Manning, A. J., Myhre, C. L., Lanoisellé, M. and Nisbet, E. G.: Measurements of δ^{13}C in CH_4 and using particle dispersion modeling to characterize sources of Arctic methane within an air mass, J. Geophys. Res. Atmos., 121(23), 14,257-14,270, doi:10.1002/2016JD026006, 2016.

France, J. L., Bateson, P., Dominutti, P., Allen, G., Andrews, S., Bauguitte, S., Coleman, M., Lachlan-Cope, T., Fisher, R. E., Huang, L., Jones, A. E., Lee, J., Lowry, D., Pitt, J., Purvis, R., Pyle, J., Shaw, J., Warwick, N., Weiss, A., Wilde, S.,

975 Witherstone, J. and Young, S.: Facility level measurement of offshore oil and gas installations from a medium-sized airborne platform: Method development for quantification and source identification of methane emissions, Atmos. Meas. Tech., 14(1), 71–88, doi:10.5194/amt-14-71-2021, 2021.

Ginty, E. M.: Carbon Isotopic Evidence That Coal Derived Methane Is Altering The Chemistry of The Global Atmosphere, Honours thesis, The University of New South Wales, Australia, 63 pp., 2016.

980 Godwin, S., Kang, A., Gulino, L.-M., Manefield, M., Gutierrez-Zamora, M.-L., Kienzle, M., Ouwerkerk, D., Dawson, K. and Klieve, A. V: Investigation of the microbial metabolism of carbon dioxide and hydrogen in the kangaroo foregut by stable isotope probing, ISME J. 2014 89, 8(9), 1855–1865, doi:10.1038/ismej.2014.25, 2014.

Gorchov Negron, A. M., Kort, E. A., Conley, S. A. and Smith, M. L.: Airborne Assessment of Methane Emissions from Offshore Platforms in the U.S. Gulf of Mexico, Environ. Sci. Technol., 54(8), 5112–5120, doi:10.1021/acs.est.0c00179, 985   2020.

Hamilton, S. K., Golding, S. D., Baublys, K. A. and Esterle, J. S.: Stable isotopic and molecular composition of desorbed coal seam gases from the Walloon Subgroup, eastern Surat Basin, Australia, Int. J. Coal Geol., 122, 21–36, doi:10.1016/j.coal.2013.12.003, 2014.

Hamilton, S. K., Golding, S. D., Baublys, K. A. and Esterle, J. S.: Conceptual exploration targeting for microbially enhanced 990   coal bed methane (MECoM) in the Walloon Subgroup, eastern Surat Basin, Australia, Int. J. Coal Geol., 138, 68–82, doi:10.1016/j.coal.2014.12.002, 2015.

Hamilton SK, Esterle JS, Golding SD.: Geological interpretation of gas content trends, Walloon Subgroup, eastern Surat Basin, Queensland, Australia. *Int. J. Coal Geol.* **101**, 21–35. doi:10.1016/j.coal.2012.07.001, 2012

Han, P., Zeng, N., Oda, T., Lin, X., Crippa, M., Guan, D., Janssens-Maenhout, G., Ma, X., Liu, Z., Shan, Y., Tao, S., Wang, 995   H., Wang, R., Wu, L., Yun, X., Zhang, Q., Zhao, F. and Zheng, B.: Evaluating China's fossil-fuel CO2 emissions from a comprehensive dataset of nine inventories, Atmos. Chem. Phys., 20(19), 11371–11385, doi:10.5194/ACP-20-11371-2020, 2020.

IPCC: Guidelines for National Greenhouse Gas Inventories (NGHGI). [online] Available from: https://www.ipcc-nggip.iges.or.jp/public/2006gl/index.html (Accessed 23 August 2021), 2006.

1000 IPCC: Refinement to the 2006 IPCC Guidelines for National Greenhouse Gas Inventories. [online] Available from: https://www.ipcc.ch/report/2019-refinement-to-the-2006-ipcc-guidelines-for-national-greenhouse-gas-inventories/ (Accessed 23 August 2021), 2019.

Iverach, C. P., Cendón, D. I., Hankin, S. I., Lowry, D., Fisher, R. E., France, J. L., Nisbet, E. G., Baker, A., and Kelly, B.F.J.: Assessing Connectivity Between an Overlying Aquifer and a Coal Seam Gas Resource Using Methane Isotopes, 1005   Dissolved Organic Carbon and Tritium, Sci. Rep., 5, 1–11, https://doi.org/10.1038/srep15996, 2015.

Iverach, C. P., Beckmann, S., Cendón, D. I., Manefield, M., and Kelly, B. F. J.: Biogeochemical constraints on the origin of methane in an alluvial aquifer: evidence for the upward migration of methane from underlying coal measures, Biogeosciences, 14, 215–228, https://doi.org/10.5194/bg-14-215-2017, 2017.

Jemena: Darling Downs Pipeline, [online] Available from: https://jemena.com.au/pipelines/darling-downs-pipeline 1010   (Accessed 29 August 2021), 2021.

Johnson MR, Tyner DR, Conley S, Schwietzke S, Zavala-Araiza D.: Comparisons of airborne measurements and inventory estimates of methane emissions in the Alberta upstream oil and gas sector. *Environ. Sci. Technol.* **51**, 13008–13017. doi:10.1021/acs.est. 7b03525, 2017

Karion, A., Sweeney, C., Pétron, G., Frost, G., Michael Hardesty, R., Kofler, J., Miller, B. R., Newberger, T., Wolter, S., 1015   Banta, R., Brewer, A., Dlugokencky, E., Lang, P., Montzka, S. A., Schnell, R., Tans, P., Trainer, M., Zamora, R. and Conley, S.: Methane emissions estimate from airborne measurements over a western United States natural gas field, Geophys. Res. Lett., 40(16), 4393–4397, doi:10.1002/grl.50811, 2013.

Karion, A., Sweeney, C., Kort, E. A., Shepson, P. B., Brewer, A., Cambaliza, M., Conley, S. A., Davis, K., Deng, A., Hardesty, M., Herndon, S. C., Lauvaux, T., Lavoie, T., Lyon, D., Newberger, T., Pétron, G., Rella, C., Smith, M., 1020   Wolter, S., Yacovitch, T. I. and Tans, P.: Aircraft-Based Estimate of Total Methane Emissions from the Barnett Shale Region, Environ. Sci. Technol., 49(13), 8124–8131, doi:10.1021/acs.est.5b00217, 2015.

Keeling, C. D.: The concentration and isotopic abundances of carbon dioxide in rural and marine air, Geochim. Cosmochim. Acta, 24(3–4), 277–298, doi:10.1016/0016-7037(61)90023-0, 1961.

Kirschke, S., Bousquet, P., Ciais, P., Saunois, M., Canadell, J. G., Dlugokencky, E. J., Bergamaschi, P., Bergmann, D., 1025   Blake, D. R., Bruhwiler, L., Cameron-Smith, P., Castaldi, S., Chevallier, F., Feng, L., Fraser, A., Heimann, M., Hodson, E. L., Houweling, S., Josse, B., Fraser, P. J., Krummel, P. B., Lamarque, J.-F., Langenfelds, R. L., Le Quéré, C., Naik, V., Palmer, P. I., Pison, I., Plummer, D., Poulter, B., Prinn, R. G., Rigby, M., Ringeval, B., Santini, M., Schmidt, M., Shindell, D. T., Simpson, I. J., Spahni, R., Paul Steele, L., Strode, S. A., Sudo, K., Szopa, S., van der Werf, G. R., Voulgarakis, A., van Weele, M., Weiss, R. F., Williams, J. E. and Zeng, G.: Three decades of global methane sources and 1030   sinks, Nat. Publ. Gr., 6, doi:10.1038/NGEO1955, 2013.

Lan, X., Basu, S., Schwietzke, S., Bruhwiler, L. M. P., Dlugokencky, E. J., Michel, S. E., Sherwood, O. A., Tans, P. P., Thoning, K., Etiope, G., Zhuang, Q., Liu, L., Oh, Y., Miller, J. B., Pétron, G., Vaughn, B. H. and Crippa, M.: Improved Constraints on Global Methane Emissions and Sinks Using δ^{13}C-CH$_4$, Global Biogeochem. Cycles, 35(6), e2021GB007000, doi:10.1029/2021GB007000, 2021.

1035 Lowry, D., Fisher, R. E., France, J. L., Coleman, M., Lanoisellé, M., Zazzeri, G., Nisbet, E. G., Shaw, J. T., Allen, G., Pitt, J. and Ward, R. S.: Environmental baseline monitoring for shale gas development in the UK: Identification and geochemical characterisation of local source emissions of methane to atmosphere, Sci. Total Environ., 708, 134600, doi:10.1016/j.scitotenv.2019.134600, 2020.

Lu, D., Ye., M., Hill, M.C.: Analysis of regression confidence intervals and Bayesian credible intervals for uncertainty 1040   quantification. Water Resources Research, Vol. 48, W09521, doi:10.1029/2011WR011289, 2012

Lu, X., Harris, S. J., Fisher, R. E., France, J. L., Nisbet, E. G., Lowry, D., Röckmann, T., Van Der Veen, C., Menoud, M.,

Schwietzke, S. and Kelly, B. F. J.: Isotopic signatures of major methane sources in the coal seam gas fields and adjacent agricultural districts, Queensland, Australia, Atmos. Chem. Phys., 21(13), 10527–10555, doi:10.5194/acp-21-10527-2021, 2021.

1045   Menoud, M., van der Veen, C., Scheeren, B., Chen, H., Szénási, B., Morales, R. P., Pison, I., Bousquet, P., Brunner, D. and Röckmann, T.: Characterisation of methane sources in Lutjewad, The Netherlands, using quasi-continuous isotopic composition measurements, Tellus, Ser. B Chem. Phys. Meteorol., 72(1), 1–19, doi:10.1080/16000889.2020.1823733, 2020.

1050   Menoud, M., van der Veen, C., Necki, J., Bartyzel, J., Szénási, B., Stanisavljević, M., Pison, I., Bousquet, P. and Röckmann, T.: Measurement report: Methane (CH4) sources in Krakow, Poland: insights from isotope analysis, Atmos. Chem. Phys. Discuss., 1–31, doi:10.5194/ACP-2021-146, 2021.

Menoud, M., van der Veen, C., Lowry, D., Fernandez, J.M., Bakkaloglu, S., France, J.L., Fisher, R.E., Maazallahi1, H., Stanisavljevi, M., Jarosław Necki, J., Vinkovic, K., Łakomiec, P., Rinne, J., Korbe, P., Schmidt, M., Defratyka, S., Yver-Kwok, C., Andersen, T., Chen, H., and Röckmann, T.: Global inventory of the stable isotopic composition of methane 1055   surface emissions, augmented by new measurements in Europe. Earth System Science Data, Discussion Preprint. Discussion started: 27 January 2022 https://doi.org/10.5194/essd-2022-30, 2022a

Menoud, M., van der Veen, C., Maazallahi, H., Hensen, A., Velzeboer, I., van den Bulk, P., Delre, A., Korben, P., Schwietzke, S., Ardelean, M., Calcan, A., Etiope, G., Baciu, C., Scheutz, C., Schmidt, M., and Röckmann, T.: CH$_4$

1060   isotopic signatures of emissions from oil and gas extraction sites in Romania, submitted to Elementa, Science of the Antropocene. (under review), 2022b

Mielke-Maday, I., Schwietzke, S., Yacovitch, T.I., Miller, B., Conley, S., Kofler, J., Handley, P., Thorley, E., Herndon, S.C., Hall, B., Dlugokencky, E., Lang, P., Wolter, S., Moglia, E., Crotwell, M., Crotwell, A., Rhodes, M., Kitzis, D., Vaughn, T., Bell, C., Zimmerle, D., Schnell, R., Pétron G.,: Methane source attribution in a U.S. dry gas basin using spatial patterns of ground and airborne ethane and methane measurements. *Elementa* 7, 351, doi:10.1525/elementa.351, 2019

1065   Milkov, A. V. and Etiope, G.: Revised genetic diagrams for natural gases based on a global dataset of >20,000 samples, Org. Geochem., 125, 109–120, doi:10.1016/J.ORGGEOCHEM.2018.09.002, 2018.

Miller, J.B., and Tans, P.P.: Calculating isotopic fractionation from atmospheric measurements at various scales. Tellus, 55B, 207 214, https://doi.org/10.1034/j.1600-0889.2003.00020.x, 2003.

Neininger, B. G., Kelly, B. F. J., Hacker, J. M., Lu, X. and Schwietzke, S.: Coal seam gas industry methane emissions in the 1070   Surat Basin , Australia: Comparing airborne measurements with inventories, Phil. Trans. R. Soc. A., Rev., 379(20200458), doi:10.1098/rsta.2020.0458, 2021.

Pataki, D. E., Ehleringer, J. R., Flanagan, L. B., Yakir, D., Bowling, D. R., Still, C. J., Buchmann, N., Kaplan, J. O. and Berry, J. A.: The application and interpretation of Keeling plots in terrestrial carbon cycle research, Global Biogeochem. Cycles, 17(1), 1022, doi:10.1029/2001GB001850, 2003.

1075   Peischl, J., Ryerson, T. B., Aikin, K. C., De Gouw, J. A., Gilman, J. B., Holloway, J. S., Lerner, B. M., Nadkarni, R., Neuman, J. A., Nowak, J. B., Trainer, M., Warneke, C. and Parrish, D. D.: Quantifying atmospheric methane emissions from the Haynesville, Fayetteville, and northeastern Marcellus shale gas production regions, J. Geophys. Res., 120(5), 2119–2139, doi:10.1002/2014JD022697, 2015.

Peischl, J., Karion, A., Sweeney, C., Kort, E. A., Smith, M. L., Brandt, A. R., Yeskoo, T., Aikin, K. C., Conley, S. A., 1080   Gvakharia, A., Trainer, M., Wolter, S. and Ryerson, T. B.: Quantifying atmospheric methane emissions from oil and natural gas production in the Bakken shale region of North Dakota, J. Geophys. Res. Atmos., 121(10), 6101–6111, doi:10.1002/2015JD024631, 2016.

Peischl, J., Eilerman, S. J., Neuman, J. A., Aikin, K. C., de Gouw, J., Gilman, J. B., Herndon, S. C., Nadkarni, R., Trainer, M., Warneke, C. and Ryerson, T. B.: Quantifying Methane and Ethane Emissions to the Atmosphere From Central and 1085   Western U.S. Oil and Natural Gas Production Regions, J. Geophys. Res. Atmos., 123(14), 7725–7740, doi:10.1029/2018JD028622, 2018.

Pétron, G., Karion, A., Sweeney, C., Miller, B. R., Montzka, S. A., Frost, G. J., Trainer, M., Tans, P., Andrews, A., Kofler, J., Helmig, D., Guenther, D., Dlugokencky, E., Lang, P., Newberger, T., Wolter, S., Hall, B., Novelli, P., Brewer, A., Conley, S., Hardesty, M., Banta, R., White, A., Noone, D., Wolfe, D. and Schnell, R.: A new look at methane and 1090   nonmethane hydrocarbon emissions from oil and natural gas operations in the Colorado Denver-Julesburg Basin, J. Geophys. Res., 119(11), 6836–6852, doi:10.1002/2013JD021272, 2014.

QGC: Surat North Development Water Resource Monitoring and Management Plan, Stage 3Water Monitoring and Management Plane, Chapter 14: Associated Water Management. [online] Available from: https://www.shell.com.au/about-us/projects-and-locations/qgc/environment/water-management/reports.html (Accessed 1095   27 Feb 2022), 2013.

Quay, P., Stutsman, J., Wilbur, D., Snover, A., Dlugokencky, E. and Brown, T.: The isotopic composition of atmospheric methane, Global Biogeochem. Cycles, 13(2), 445–461, doi:10.1029/1998GB900006, 1999.

Röckmann, T., Eyer, S., Van Der Veen, C., Popa, M. E., Tuzson, B., Monteil, G., Houweling, S., Harris, E., Brunner, D., Fischer, H., Zazzeri, G., Lowry, D., Nisbet, E. G., Brand, W. A., Necki, J. M., Emmenegger, L. and Mohn, J.: In situ 1100   observations of the isotopic composition of methane at the Cabauw tall tower site, Atmos. Chem. Phys, 16, 10469–10487, doi:10.5194/acp-16-10469-2016, 2016.

Saunois, M., R. Stavert, A., Poulter, B., Bousquet, P., G. Canadell, J., B. Jackson, R., A. Raymond, P., J. Dlugokencky, E., Houweling, S., K. Patra, P., Ciais, P., K. Arora, V., Bastviken, D., Bergamaschi, P., R. Blake, D., Brailsford, G., Bruhwiler, L., M. Carlson, K., Carrol, M., Castaldi, S., Chandra, N., Crevoisier, C., M. Crill, P., Covey, K., L. Curry, C., 1105   Etiope, G., Frankenberg, C., Gedney, N., I. Hegglin, M., Höglund-Isaksson, L., Hugelius, G., Ishizawa, M., Ito, A.,

Janssens-Maenhout, G., M. Jensen, K., Joos, F., Kleinen, T., B. Krummel, P., L. Langenfelds, R., G. Laruelle, G., Liu, L., MacHida, T., Maksyutov, S., C. McDonald, K., McNorton, J., A. Miller, P., R. Melton, J., Morino, I., Müller, J., Murguia-Flores, F., Naik, V., Niwa, Y., Noce, S., O'Doherty, S., J. Parker, R., Peng, C., Peng, S., P. Peters, G., Prigent,
1110   C., Prinn, R., Ramonet, M., Regnier, P., J. Riley, W., A. Rosentreter, J., Segers, A., J. Simpson, I., Shi, H., J. Smith, S., Paul Steele, L., F. Thornton, B., Tian, H., Tohjima, Y., N. Tubiello, F., Tsuruta, A., Viovy, N., Voulgarakis, A., S. Weber, T., Van Weele, M., R. Van Der Werf, G., F. Weiss, R., Worthy, D., Wunch, D., Yin, Y., Yoshida, Y., Zhang, W., Zhang, Z., Zhao, Y., Zheng, B., Zhu, Q., Zhu, Q. and Zhuang, Q.: The global methane budget 2000-2017, Earth Syst. Sci. Data, 12(3), 1561–1623, doi:10.5194/essd-12-1561-2020, 2020.

Schwietzke, S., Pétron, G., Conley, S., Pickering, C., Mielke-Maday, I., Dlugokencky, E. J., Tans, P. P., Vaughn, T., Bell,
1115   C., Zimmerle, D., Wolter, S., King, C. W., White, A. B., Coleman, T., Bianco, L. and Schnell, R. C.: Improved Mechanistic Understanding of Natural Gas Methane Emissions from Spatially Resolved Aircraft Measurements, Environ. Sci. Technol., 51(12), 7286–7294, doi:10.1021/acs.est.7b01810, 2017.

Scott, S., Anderson, B., Crosdale, P., Dingwall, J. and Leblang, G.: Coal petrology and coal seam gas contents of the Walloon Subgroup — Surat Basin, Queensland, Australia, Int. J. Coal Geol., 70(1–3), 209–222,
1120   doi:10.1016/J.COAL.2006.04.010, 2007.

Sherwood, O. A., Schwietzke, S., Arling, V. A. and Etiope, G.: Global Inventory of Gas Geochemistry Data from Fossil Fuel, Microbial and Burning Sources, version 2017, Earth Syst. Sci. Data, 9, 639–656, doi:10.5194/essd-9-639-2017, 2017.

Sherwood, O. A., Schwietzke, S. and Lan, X.: Global δ 13 C-CH4 Source Signature Inventory 2020. [online] Available
1125   from: https://doi.org/10.15138/qn55-e011(Accessed 27 Feb 2022), 2020.

Smit, S.: MultiNonlinearModelFit., Wolfram Function Repository. [online] Available from: https://resources.wolframcloud.com/FunctionRepository/resources/MultiNonlinearModelFit. (Accessed 27 Jan 2022), 1986.

Smith ML, Kort EA, Karion A, Sweeney C, Herndon SC, Yacovitch TI.: Airborne ethane observations in the Barnett Shale:
1130   quantification of ethane flux and attribution of methane emissions. *Environ. Sci. Technol.* **49**, 8158–8166. doi:10.1021/acs.est.5b00219, 2015

Stalker, L. and Smith, J. K.: Stable Carbon Isotope Analysis of a Gas Sample From The MT LINDESAY-1 Well, Bentley, WA 6102, Australia., 2004.

Stein, A. F., Draxler, R. R., Rolph, G. D., Stunder, B. J. B., Cohen, M. D. and Ngan, F.: NOAA's HYSPLIT Atmospheric
1135   Transport and Dispersion Modeling System, Bull. Am. Meteorol. Soc., 96(12), 2059–2077, doi:10.1175/BAMS-D-14-00110.1, 2015.

Tarasova, O. A., Brenninkmeijer, C. A. M., Assonov, S. S., Elansky, N. F., Röckmann, T. and Brass, M.: Atmospheric CH4 along the Trans-Siberian railroad (TROICA) and river Ob: Source identification using stable isotope analysis, Atmos. Environ., 40(29), 5617–5628, doi:10.1016/j.atmosenv.2006.04.065, 2006.

1140   Townsend-Small, A., Marrero, J. E., Lyon, D. R., Simpson, I. J., Meinardi, S. and Blake, D. R.: Integrating Source Apportionment Tracers into a Bottom-up Inventory of Methane Emissions in the Barnett Shale Hydraulic Fracturing Region, Environ. Sci. Technol., 49(13), 8175–8182, doi:10.1021/acs.est.5b00057, 2015.

Turner, A. J., Jacob, D. J., Wecht, K. J., Maasakkers, J. D., Lundgren, E., Andrews, A. E., Biraud, S. C., Boesch, H., Bowman, K. W., Deutscher, N. M., Dubey, M. K., Griffith, D. W. T., Hase, F., Kuze, A., Notholt, J., Ohyama, H.,
1145   Parker, R., Payne, V. H., Sussmann, R., Sweeney, C., Velazco, V. A., Warneke, T., Wennberg, P. O. and Wunch, D.: Estimating global and North American methane emissions with high spatial resolution using GOSAT satellite data, Atmos. Chem. Phys, 15, 7049–7069, doi:10.5194/acp-15-7049-2015, 2015.

Verhulst, K. R., Karion, A., Kim, J., Salameh, P. K., Keeling, R. F., Newman, S., Miller, J., Sloop, C., Pongetti, T., Rao, P., Wong, C., Hopkins, F. M., Yadav, V., Weiss, R. F., Duren, R. M. and Miller, C. E.: Carbon dioxide and methane
1150   measurements from the Los Angeles Megacity Carbon Project-Part 1: calibration, urban enhancements, and uncertainty estimates, Atmos. Chem. Phys, 17, 8313–8341, doi:10.5194/acp-17-8313-2017, 2017.

Whiticar, M. J.: Carbon and hydrogen isotope systematics of bacterial formation and oxidation of methane, Chem. Geol., 161(1), 291–314, doi:10.1016/S0009-2541(99)00092-3, 1999.

WMO: GAW Report No. 255. 20th WMO/IAEA Meeting on Carbon Dioxide, Other Greenhouse Gases and Related
1155   Measurement Techniques (GGMT-2019), Jeju Island, South Korea. [online] Available from: https://library.wmo.int/doc_num.php?explnum_id=10353 (Accessed 9 April 2021), 2020.

Wolfram Research Inc.: Mathematica Version 12.0, Champaign, Illinois [online] Available from: https://www.wolfram.com/mathematica (Accessed 17 January 2022), 2019.

Worden, J. R., Bloom, A. A., Pandey, S., Jiang, Z., Worden, H. M., Walker, T. W., Houweling, S. and Röckmann, T.:
1160   Reduced biomass burning emissions reconcile conflicting estimates of the post-2006 atmospheric methane budget, Nat. Commun., 8(1), 1–11, doi:10.1038/s41467-017-02246-0, 2017.

Yacovitch, T. I., Neininger, B., Herndon, S. C., van der Gon, H. D., Jonkers, S., Hulskotte, J., Roscioli, J. R. and Zavala-Araiza, D.: Methane emissions in the Netherlands: The Groningen field, Elem. Sci. Anthr., 6, 57, doi:10.1525/ELEMENTA.308, 2018.

1165   Zazzeri, G., Lowry, D., Fisher, R. E., France, J. L., Lanoisellé, M., Grimmond, C. S. B. and Nisbet, E. G.: Evaluating methane inventories by isotopic analysis in the London region, Sci. Rep., 7(1), doi:10.1038/S41598-017-04802-6, 2017.

Zhang, Y., Gautam, R., Pandey, S., Omara, M., Maasakkers, J. D., Sadavarte, P., Lyon, D., Nesser, H., Sulprizio, M. P., Varon, D. J., Zhang, R., Houweling, S., Zavala-Araiza, D., Alvarez, R. A., Lorente, A., Hamburg, S. P., Aben, I. and Jacob, D. J.: Quantifying methane emissions from the largest oil-producing basin in the United States from space, Sci.

1170 Adv., 6(17), 1–10, doi:10.1126/sciadv.aaz5120, 2020.

Zhang, Y., J. Jacob, D., Lu, X., D. Maasakkers, J., R. Scarpelli, T., Sheng, J. X., Shen, L., Qu, Z., P. Sulprizio, M., Chang, J., Anthony Bloom, A., Ma, S., Worden, J., J. Parker, R. and Boesch, H.: Attribution of the accelerating increase in atmospheric methane during 2010-2018 by inverse analysis of GOSAT observations, Atmos. Chem. Phys., 21(5), 3643–3666, doi:10.5194/ACP-21-3643-2021, 2021.

1175